2D Variational Ambiguity Removal

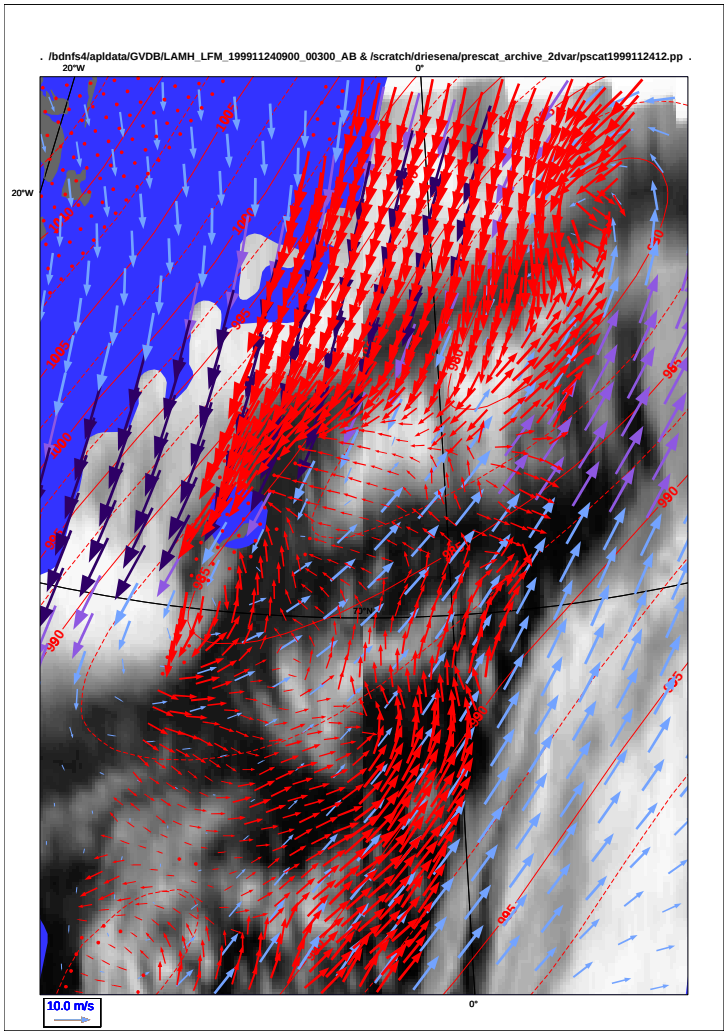

John de Vries, Ad Stoffelen

February 2000

Abstract

We explain the workings of existing methods for ambiguity removal and describe in detail how we use the known spatial structure of the synoptic scale wind field, as used in meteorological analysis, to improve ambiguity removal skill in a new scheme called 2D-VAR.

2D-VAR is a variational scheme that solves the ambiguity removal problem by minimizing a cost function. The cost function is formulated in terms of wind increments and penalizes deviations from both a background wind field and the ambiguous scatterometer wind solutions obtained from ERS scatterometer wind retrieval.

A main feature of 2D-VAR is the use of a discrete grid that extends beyond the scatterometer swath to incorporate wind increments, generated outside the swath due to scatterometer observations near or at the edge of the swath. The wind increments contribute to the cost function and help to obtain a realistic and meteorologically consistent solution. Another feature of 2D-VAR is observation grouping which appoints a mean location to a group of retrieved ambiguous scatterometer winds. This has the effect of observation smoothing that appears to have a beneficial effect in areas with large gradients (fronts).

Validation of its performance shows that 2D-VAR has both strengths and weaknesses. An objective comparison with PRESCAT, a state-of-the-art ambiguity removal scheme, favours PRESCAT. Subjective analysis by meteorologists at KNMI favours 2D-VAR for cases were 2D-VAR and PRESCAT give significantly different solutions.

2D-VAR will be compared to similar schemes in the framework of the Ocean and Sea Ice Satellite Application Facility to assess its suitability for implementation in the SAF processing chain. In the near future, at KNMI, 2D-VAR will be used for the ambiguity removal of QuikSCAT winds.

Contents

List of Figures

Executive Summary

Scatterometers are satellite-based active microwave remote sensors that can well depict the near-surface wind field over water. However the information obtained on wind direction is not unique. After ERS scatterometer wind retrieval two ambiguous wind vector solutions emerge. These two wind vectors are approximately 180^0 apart in wind direction. Obviously only one of the wind vectors is physically correct. The correct ambiguity has to be selected in a way that will produce a meteorologically consistent wind field. The process to achieve this is called ambiguity removal (AR).

With todays skill in ambiguity removal in about 99% of cases a consistent wind field is obtained. However in highly dynamical situations current AR-schemes often give solutions that are meteorologically inconsistent. This is unfortunate because scatterometer observations potentially have added value in situations of large atmospheric variability. To improve AR-skill we use the known spatial structure of the synoptic scale wind field in a scheme called 2D-VAR to correct errors in a background wind field and obtain a meteorologically consistent wind field that is a weighted average of the background information and scatterometer observations. This approach is different from that of current AR-schemes which are purely statistical in nature.

The 2D-VAR scheme is described mathematically as an unconstrained minimisation of the wind increments. The cost function to be minimised is defined as the sum of a background term and an observational term. The background term penalizes deviations from a 3 hour forecast of the 10 m wind. The forecast time for the 10m wind can differ up to 1.5 hours from the time of observation. The observational term expresses the ambiguity involved in the wind vector solutions and prescribes the penalty at each observation point for deviating from either of the ambiguous wind vectors obtained from the wind retrieval. The minimisation is an iterative proces during which observational information is spread spatially by means of so-called structure functions. It is these structure functions that incorporate our knowledge of the physical laws that constrain the spatial structure of the synoptic wind. In the 2D-VAR analysis the optimal solution for the wind increments is obtained on a discrete square grid that extends outside the area that encloses the scatterometer observations known as the 'swath'. This extention enables 2D-VAR to also apply

a penalty to wind increments that are spread, by the structure functions, outside the swath. This way the solution is realistically constrained for observations near or at the edge of the scatterometer swath in accordance with the known spatial error structure of the 3 hour forecast wind field. 2D-VAR implements a feature called observation grouping. Groups of ambiguous wind vector pairs are collocated in a mean location which has the effect of spatial smoothing of observational information. A case is presented that indicates that smoothing of observational information may have a beneficial effect on the wind analysis near fronts.

In comparison with current state-of-the-art AR-schemes, i.c. PRESCAT, 2D-VAR exhibits both strengths and weaknesses after our performance validation. We executed an objective test that compared 2D-VAR and PRESCAT in terms of wind vector difference with an absolute reference. On average this resulted in a better score for PRESCAT. A complementary subjective analysis was carried out by KNMI meteorologists. In this analysis, meteorologists compared wind products based on the same observations but with different methods for ambiguity removal (2D-VAR versus PRESCAT). The comparison was done for cases where the wind products were significantly different. In the comparison meteorologists used independent information and their expertise to determine which of the wind products was best in their view. The analysis favoured 2D-VAR. Findings of the meteorologists and case studies show that 2D-VAR is successful in removing the 180^0 ambiguity in surface winds for small-scale weather systems, provided it seems that the scale of the systems matches that of the structure functions. The behaviour of 2D-VAR in data-sparse situations is not optimal which remains an issue of concern.

2D-VAR is a useful tool that will be developed further. Apart from improving its behaviour in data-sparse situations, the investigation into the use of situation-dependent structure functions may be worthwhile. 2D-VAR will be compared to similar schemes in the framework of the Ocean and Sea Ice Satellite Application Facility to assess its suitability for implementation in the SAF processing chain. In the near future, at KNMI, 2D-VAR will be used for the ambiguity removal of QuikSCAT data.

Preface

The 2D-VAR project has been jointly funded by KNMI and the Netherlands Remote Sensing Board (BCRS). BCRS funding was approved under the User Support Programme. The project started in September of 1997 and was carried out at KNMI in De Bilt (Netherlands).

The 2D Variational Ambiguity Removal (2D-VAR) project has been carried out in the framework of the Ocean and Sea Ice Satellite Application Facility (OSI SAF) project (*http://www.eumetsat.de/*). The OSI SAF is sponsored by EUMETSAT and aims to establish an operational processing system for the generation of a surface wind vector product. This OSI SAF processing system consists of several modules that perform the necessary steps, such as inversion, ice screening, ambiguity removal, monitoring etc., to obtain, among others, a wind product suitable for meteorological and other, related applications. The wind product is based on measurements from the ERS-scatterometer and in the future from METOP/ASCAT.

Acknowledgement: The authors wish to thank Tilly Driesenaar for her work in building the infrastructure on the Web to view wind products on-line. This made it possible to carry out the 2D-VAR/PRESCAT comparison study by meteorologists. We also want to thank the meteorologists at KNMI for their input and enthousiasm during the subjective validation.

Acronyms

2D-VAR	2D Variational Ambiguity Removal
ASCAT	Advanced Scatterometer on METOP
AR	Ambiguity Removal
ECMWF	European Centre for Medium-Range Weather Forecasting
EPS	European Polar System
ERS	ESA Remote Sensing satellite
ESA	European Space Agency
EUMETSAT	European Organisation for Meteorological Satellites
FFT	Fast Fourier Transform
FGAT	First Guess at Appropriate Time
HIRLAM	High Resolution Limited Area Model
METOP	Meteorological Operational Satellite
NWP	Numerical Weather Prediction
OSI SAF	Ocean and Sea Ice Satellite Application Facility
PRESCAT	Pre-processor for ERS Scatterometer data
SCAT	ERS scatterometer

Chapter 1

Introduction

Scatterometers are satellite-based active microwave remote sensors that have the unique ability to determine the near-surface wind speed and direction over water. The scatterometer wind observations have a variety of applications among which is weather forecasting. A surface wind vector product based on scatterometer observations can be used in the nowcasting of storms for instance. The process of generating a unique and high-quality wind product involves several steps. One of the steps is ambiguity removal.

To give some background on what ambiguity removal is, on its history, the current state of affairs and how the skill in ambiguity removal might be improved upon, a brief overview is given of the use of scatterometer observations. For a more in depth and complete treatment of the subject of scatterometry the reader is referred to Stoffelen [14].

1.1 The ERS-scatterometer

The ESA remote sensing satellites, ERS-1 and ERS-2, were launched in 1991 and 1995 respectively. They both circle the Earth in a polar orbit of about 800 km height. The scatterometers on board ERS-1 and ERS-2 are identical and have three antennae that illuminate the ocean surface from three different azimuthal directions (fig. 1.1) with a 5.3 GHz radar beam (C-band). The radar beam has a footprint of 50 km in diameter at the water surface where it is Bragg scattered by capillary waves. The beams illuminate an area of about 500 km wide across the satellite track known as the swath. The swath is sampled every 25 km in both along- and across-track directions. The return signals received by the three scatterometer antennae are known as backscatter triplets or σ^0's. The σ^0's are organised into messages of

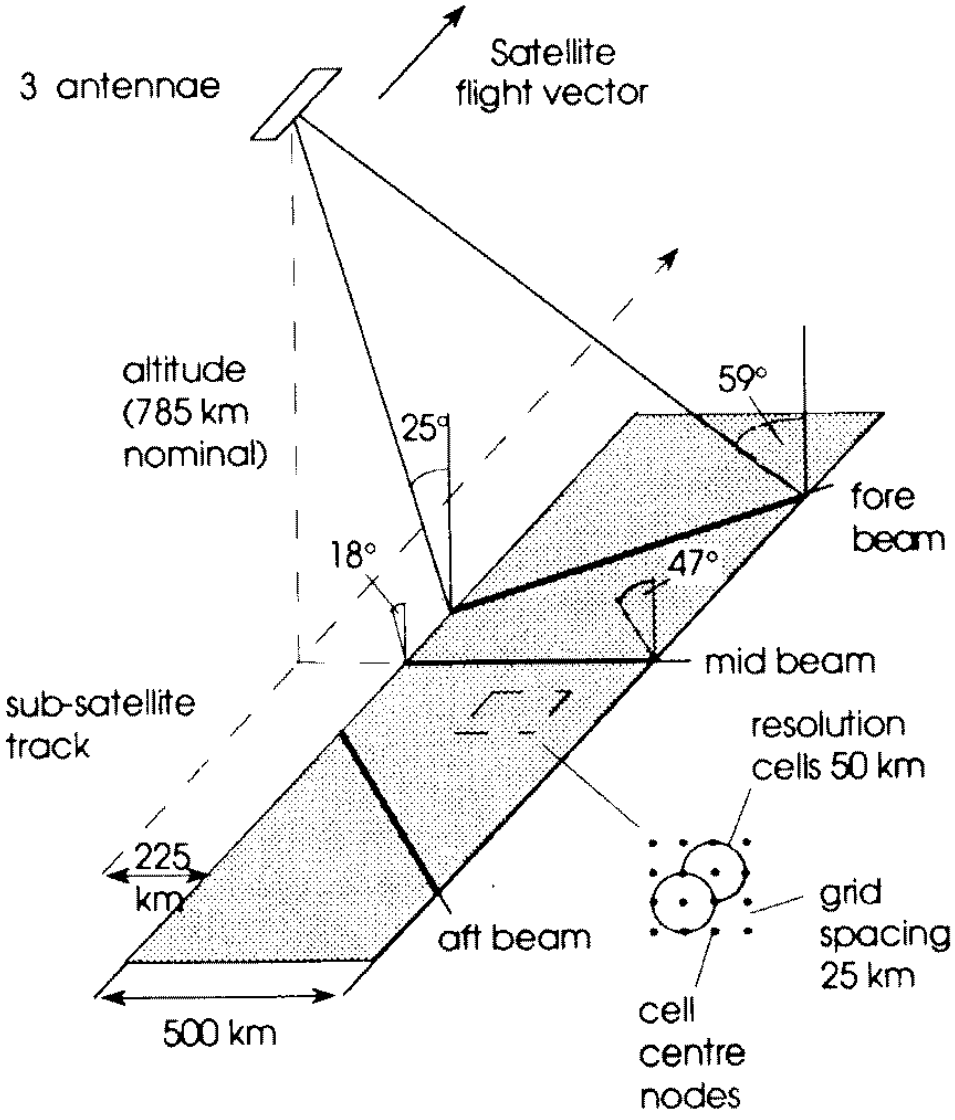

Figure 1.1: The scanning geometry of ERS scatterometers.

19x19 nodes that form a regular square grid with a 25 km grid spacing.

The backscatter triplets can be represented in a 3D measurement space with the measurement of each antenna defined along one of the three axes. The distribution of the triplets in the measurement space shows a strong coherence and the triplets are generally located near a twodimensional conical surface (fig.1.2).

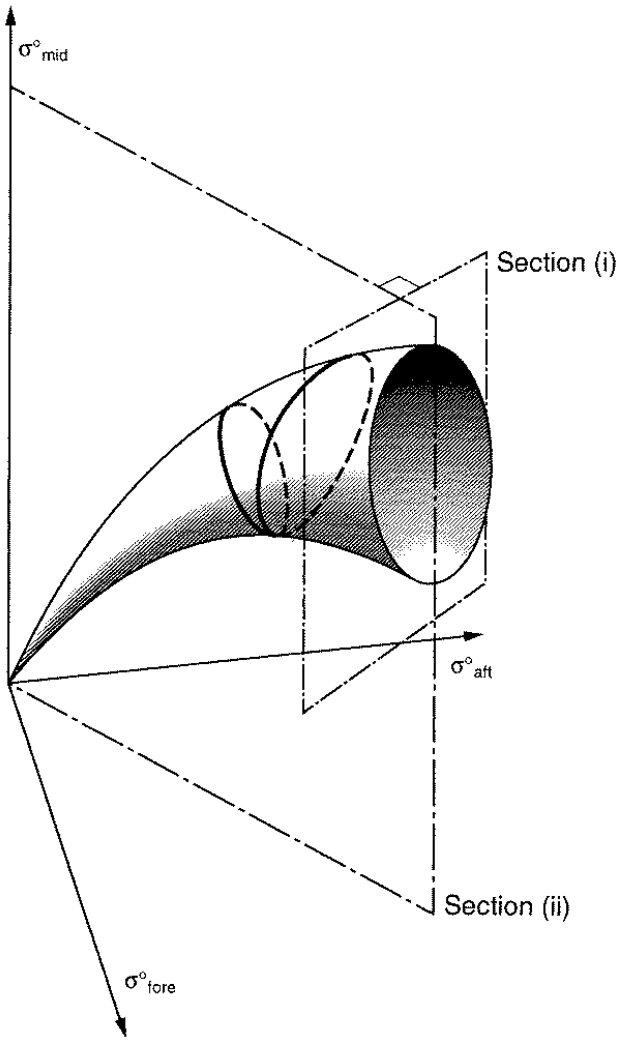

Figure 1.2: Definition of the cone in σ^0 space (from Stoffelen [14]).

It turns out that variation in the location of a triplet along the major axis of the cone, is mainly due to sea surface roughness (i.e. the size of the capillary waves), which is in turn an indirect measure of wind speed. In addition the length of the cone's minor axis is a measure of the anisotropy in the backscattering. This anisotropy is due to the orientation of the capillary waves and is strongly related to the wind direction. The wind vector is found by fitting the backscatter triplets to a microwave-wind transfer function. The speed and direction that most likely correspond to the observed backscatter triplets is called the rank 1 solution and is ideally the true wind direction. The retrieval however has multiple minima, two in the case of the ERS scatterometers. The reason for the occurence of multiple minima is because the cone surface consists of two sheaths. Physically this is due to the fact that it is not possible to distinguish between a backscatter signal received from capillary waves moving in a particular direction or in the direction opposite to that. Therefore it is not possible to find a unique solution for the wind vector.

For the retrieval of ERS wind vector solutions Stoffelen & Anderson [17] have developed an accurate backscatter-wind transfer function called CMOD4. With this transfer function noisy backscatter triplets can generally be translated into two wind vector solutions with roughly almost opposite directions (Stoffelen [15]). Either wind vector solution, if selected, is of high quality. The process of obtaining the wind solutions is called *inversion*.

To obtain a unique wind vector a selection has to be made from the retrieved wind vector solutions. The process of doing so is called *ambiguity removal*. The aim of ambiguity removal is to select the unique wind vector at each node in a way that yields a physically consistent wind field.

1.2 Current schemes for ERS Ambiguity Removal

In the past several ambiguity removal schemes have been developed for the ERS-scatterometer. Two of the most widely used schemes are described below.

CREO

Cavanie & Lecomte [3] have developed a scheme called CREO which was selected and implemented by ESA as the pre-launch ambiguity removal scheme for the ERS-1 scatterometer. CREO constructs two antiparallel fields from the wind vector solutions at each node. Subsequently it determines for both fields the number of cases in which the rank 1 solution is chosen. If this number is significantly higher for

one of the fields than the field with the higher number is selected. If this procedure is inconclusive both fields are correlated with a numerical weather-prediction (NWP) forecast for the surface wind. If the correlation is significantly higher for one of the fields than that field is selected, otherwise no solution is provided.

The application of CREO at ECMWF has lead to adequate results in about 65% of cases but in about 30% of cases CREO did not give a solution and in about 5% of cases with a complex and dynamic synoptic situation CREO presented a wrong solution. The latter is unfortunate because in those cases the scatterometer observations are potentially the most useful.

PRESCAT

The PRESCAT scheme developed by Stoffelen & Anderson [16] at ECMWF is the operational ambiguity removal scheme at KNMI and is implemented in HIRLAM (Stoffelen & Van Beukering [18]). This scheme starts by selecting the wind vector solution closest to a background field based on wind vector difference. The background field or first guess, is a short-range forecast for the 10 m wind. The initialisation results in a consistent wind field in about 95% of cases. In the remaining cases where the wind field turns out to be unmeteorological in local regions a spatial filter is applied to enhance the meteorological consistency. The way this filter works is partly based on SLICE, a filter developed by Offiler [10] which has been modified and enhanced. The filter includes a box of 5x5 nodes on the scatterometer swath that slides over the wind field. The filter computes at each node a mean likelihood for both wind vector solutions based on wind vector consistency within the box. The wind vectors at the neighbouring nodes are weighted by a confidence factor. At each node the wind vector solution with the highest mean likelihood is selected. After that the confidence factor at the node is updated depending on likelihood.

The filter starts at the inside of the swath and moves in the across-track direction. When the outside of the swath is reached the filter moves one row down in the along-track direction and makes a backscan. When it arrives at the last of the maximum of 114 rows it reverses direction and retraces its track. After this the procedure is repeated starting at the outside of the swath. In this way a total of 4 independent passes are made which is the minimum. Additional sets of four passes are carried out until the number of changes in the wind vector selection is less than a specific number.

Experience has shown that PRESCAT removes the ambiguity in almost 99% of cases. In practice it has however been shown to be sensitive to the quality of the

forecast wind field. Mis-positioning of low-pressure systems and/or errors in the strength of the forecast wind field relative to corresponding observations may still lead to erroneous wind vector selection in some areas of the swath. These selection errors are found to occur in meteorologically important, highly dynamic situations as can be seen in figure 1.3 for example. In this figure the observed surface wind field contains a strong vortex (left panel). The right panel shows the background wind field with a weak vortex in a different location. PRESCAT gives the wrong solution in the boxed area.

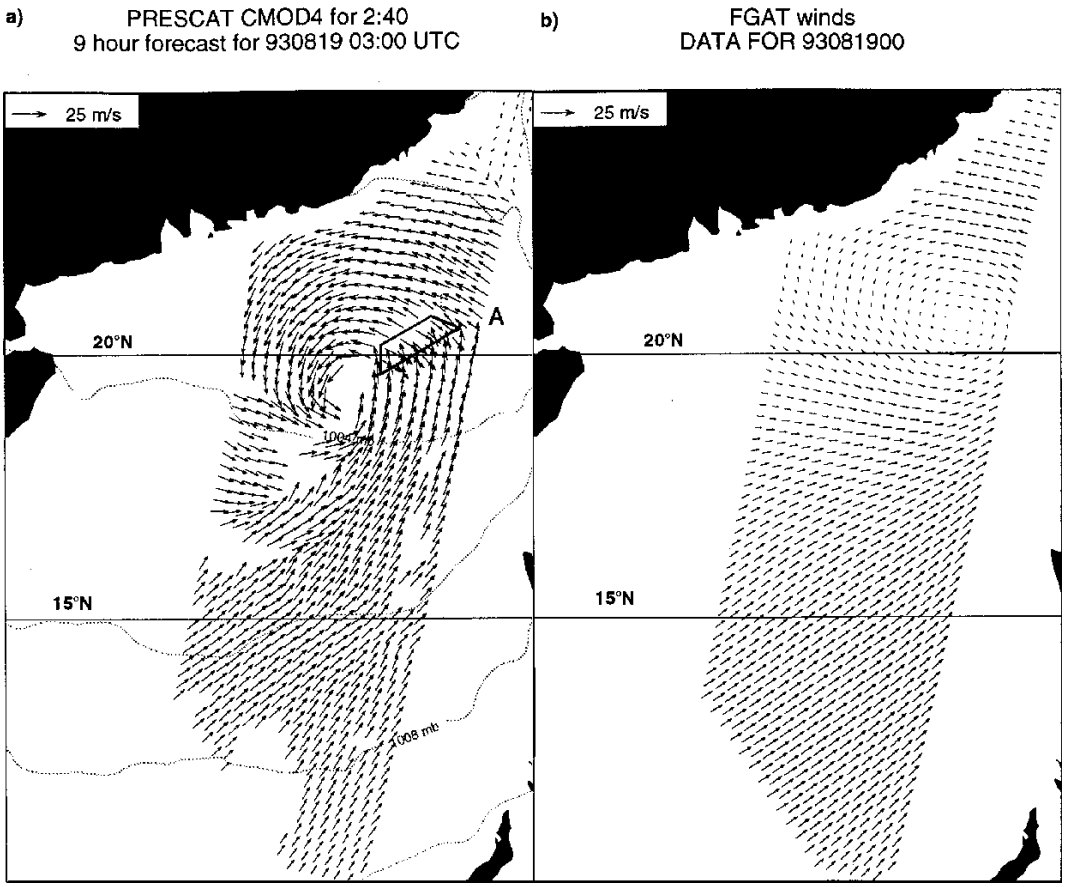

Figure 1.3: Case of erroneous wind vector selection by PRESCAT (from Stoffelen [14]).

1.3 Towards improved ambiguity removal skill

The ambiguity removal schemes described in the previous section are purely statistical in nature. A more physical (meteorological) approach would be to make use of the known spatial structure of the wind field. In the NWP analysis for the mid-latitudes the geostrophic balance between the wind field and the geopotential field provides an important constraint on the spatial structure of synoptic scale winds. An ambiguity removal scheme that uses this structure of the wind to correct errors would likely result in a meteorologically more consistent analysis of the near-surface wind field. This should lead to an improvement in ambiguity removal skill. The corrections can be applied by error covariances as is done in variational data assimilation. Fig 3.2 shows an example of the spatial error structure used in 2D-VAR.

At ECMWF both ambiguous scatterometer winds are assimilated into the global NWP model in a 6-hour cycle. The ambiguity is removed implicitly in the analysis procedure. NWP analyses however are not carried out timely and frequently enough for near real-time application of scatterometer winds. Moreover full 3D or 4D analysis are computationally expensive.

We propose therefore to implement a single level (2D) variational analysis scheme of the wind components for the ambiguity removal of the scatterometer surface wind. Such a 2D variational ambiguity removal (2D-VAR) scheme works on a grid that incorporates a stretch of the scatterometer swath (fig.1.4). The grid extends beyond the area covered by the observations to incorporate analysis increments that fall outside the bounding box. The selected ambiguity at each scatterometer node is the one closest to the 2D-VAR analysis.

The 2D-VAR scheme proposed here uses only scatterometer observations. This reduces the complexity of the scheme compared to a multivariate 3D-VAR assimilation system. Moreover using only scatterometer observations is not much of a restriction since they are the only meteorological observations available over most of the world's oceans. Because of the great spatial consistency of scatterometer observations, incorporating other types of meteorological observations would add little extra information anyway. This also implies that a 3D/4D-VAR system acts like a 2D-VAR system over the oceans.

Other AR-schemes have been developed based on meteorological data assimilatation techniques. A successive corrections ambiguity removal scheme has been implemented by Schyberg and Breivik [12]. The spatial filtering characteristics of this

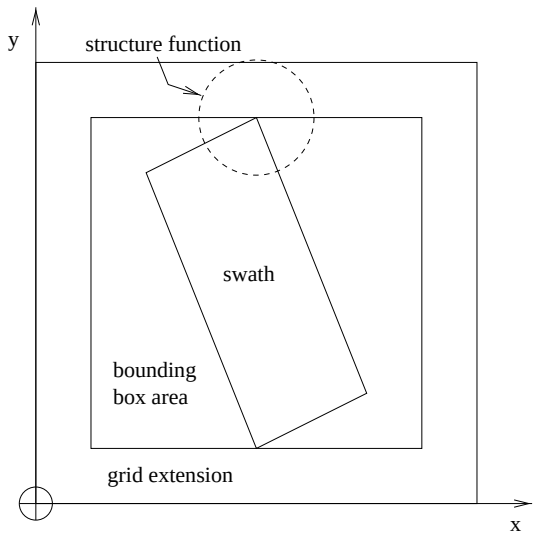

Figure 1.4: The extended grid of 2D-VAR.

scheme are similar to 2D-VAR. However the convergence properties of 2D-VAR are better and Schyberg and Breivik did not consider an extended swath. Nonetheless, they show that the AR-skill of their scheme is marginally better than the performance of PRESCAT and substantially better than CREO.

The motivation for improving ambiguity removal skill is that it potentially has added value for nowcasting and short-range weather forecasting when presenting a scatterometer wind product to a meteorologist. 2D-VAR is also an excellent tool to test the assimilation and ambiguity removal in variational analysis. This is relevant for new scatterometer systems such as NSCAT and SeaWinds, and their use in 3D and 4D-VAR. For example we tested a new method for spatial smoothing of scatterometer data to improve the spatial filtering characteristics of variational analysis (see section 2.5).

1.3.1 Overview of this report

In chapter 2 of this report a mathematical description is given of the 2D-VAR algorithm. Chapter 3 reports on the comparison of skill between 2D-VAR and PRESCAT and the application of 2D-VAR in meteorologically relevant situations. Chapter 4 discusses the skill of 2D-VAR, remaining issues and gives an outlook on future developments. Finally the appendices give a more elaborate description on computations involved in some of the issues that come up in this report.

Conventions

In the text and mathematical formulae of this report vector variables are denoted using a **bold-faced** font and lower-case characters, matrices are in **bold-faced** font and upper-case characters and for scalar variables a normal-faced font and lower-case characters are used.

Chapter 2

The 2D-VAR scheme

2.1 Variational Formulation

In a 3D/4D variational analysis scheme removal of the ambiguity in the scatterometer wind vector solution is performed implicitly. It is formulated as part of the full minimisation problem (Thépault [19] *et al.*) where the observation operator is in the wind domain as in Stoffelen & Anderson [16]. 2D-VAR is a variational analysis scheme used solely for the purpose of ambiguity removal. This variational scheme uses background information on the state of the wind field. It involves the minimisation of a cost function. This cost function expresses the aim to find the state of the near surface wind field that is most probable given the prior knowledge about it and given the ambiguous scatterometer winds. Using probability theory and Bayes Theorem this probability can be expressed as (Lorenc [8])

$$P(\mathbf{x} \cap \mathbf{v_o^i}) \propto P(\mathbf{v_o^i}|\mathbf{x}) P(\mathbf{x}|\mathbf{x_b}) \tag{2.1}$$

where

$\mathbf{x}$	is the control variable
$\mathbf{x_b}$	is the prior background information on the state of the near-surface wind field
$\mathbf{v_o^i}$	vector of scatterometer retrieved wind vector solutions
$P(\mathbf{x} \cap \mathbf{v_o^i})$	is the joint probability of the true state of the near-surface wind field $\mathbf{x}$ and the observations $\mathbf{v_o^i}$
$P(\mathbf{v_o^i}\|\mathbf{x})$	is the conditional probability that the $\mathbf{v_o^i}$ are observed given the state vector $\mathbf{x}$
$P(\mathbf{x}\|\mathbf{x_b})$	is the conditional probability that $\mathbf{x}$ is the near-surface wind field when $\mathbf{x_b}$ is the background state

and $\propto$ means 'proportional to'. The most likely estimate of $\mathbf{x}$ is found if we maximize $P(\mathbf{x} \cap \mathbf{v_o^i})$. This is equivalent to minimizing a cost function

$$J(\mathbf{x}) = -2 \ln P(\mathbf{v_o^i}|\mathbf{x}) - 2 \ln P(\mathbf{x}|\mathbf{x_b}) \tag{2.2}$$

2.2 Specification of the Cost Function

To increase the computational efficiency of 2D-VAR the analysis increments are used as controle variable in the minimization instead of the atmospheric state. The *incremental formulation* is obtained when the background field is subtracted from the state vector, i.e.

$$\delta\mathbf{x} = (\mathbf{x} - \mathbf{x_b}) = \begin{pmatrix} \mathbf{u}' \\ \mathbf{v}' \end{pmatrix} \tag{2.3}$$

and also from the wind vector solutions $\mathbf{v_o^i}$. The primes in (2.3) denote increments or departures. We will drop the primes again from the notation at this point and further describe wind increments unless explicitly stated otherwise. The cost function (2.2) in 2D-VAR becomes

$$minJ = J_o^{scat}(\mathbf{v_o^i}, \delta\mathbf{x}) + J_b(\delta\mathbf{x}) \tag{2.4}$$

The background term

For the formulation of the background term in the cost function it is assumed that the background wind field contains errors that can be characterised by a Gaussian-distributed error distribution around the wind vector components.

$$P(\delta\mathbf{x}) \propto \exp^{\frac{1}{2}(\delta\mathbf{x})^t \mathbf{B}^{-1}(\delta\mathbf{x})} \tag{2.5}$$

where $\mathbf{B}$ is the matrix of background wind error covariances. With a Gaussian distribution the background term of the cost function in incremental form becomes the quadratic form

$$J_b(\delta\mathbf{x}) = -2 \ln P(\delta\mathbf{x}) = \delta\mathbf{x}^t B^{-1} \delta\mathbf{x} + constant \tag{2.6}$$

The observational term

As with the background field the wind vector solutions contain errors, i.e. instrument errors, spatial representativeness errors and errors associated with the inversion procedure. According to Stoffelen [16] the error distribution for unambiguous

scatterometer winds is Gaussian around the vector components. Stoffelen and Anderson [16] derive for the first term of Eq.(2.2) :

$$P(\mathbf{v_o^i}|\mathbf{v}) = N(\mathbf{v_o^1}, \mathbf{e_s})/2 + N(\mathbf{v_o^2}, \mathbf{e_s})/2 \tag{2.7}$$

where N is a 2D normal distribution around the wind components $\mathbf{v_o^i}, i = 1, 2$, with width $\mathbf{e_s}$. $\mathbf{e_s} = (\varepsilon_s, \varepsilon_s)$ is the standard deviation of the expected total mean component wind error for scatterometer winds. The resulting double Gaussian observational cost term is not quadratic. For ambiguity removal it has the unfavourable characteristic that the minima are not well defined for low wind speeds and even leads to one minimum at low wind speed.

As an alternative to the double Gaussian, Stoffelen and Anderson [16] have proposed an analytical function for the cost term. In incremental form this function is defined at each observation point as

$$J_o^{scat} = -2 \ln P(\mathbf{v_o^i}|\mathbf{x}) = \left[\frac{J_1^4 J_2^4}{J_1^4 + J_2^4} \right]^{1/4} + constant \tag{2.8}$$

with

$$J_i = \frac{(H(u) - u_i)^2 + (H(v) - v_i)^2}{\varepsilon_s^2}, i = 1, 2 \tag{2.9}$$

H is the so-called observation operator which in this case is just a spatial interpolation operator that maps the state vector onto the observations. It can be seen in figure 2.1 that this function has minima at $\mathbf{v_o^i}$ and much better separation of the minima at low wind speeds.

2.3 Treatment of the background term

The 2D-VAR cost function as described in the previous section is well established. However there are several problems that have to be dealt with to obtain a practical implementation of 2D-VAR. These problems concern the size and structure of the error covariance matrix $\mathbf{B}$ in Eq.(2.6). So special care has to be taken in the evaluation of the background term J_b.

Calculation of the contribution of the background term to the cost function involves the computation of the inverse of the background error covariance matrix $\mathbf{B}$. This may give rise to two main difficulties. First of all $\mathbf{B}$ has to be non-singular in order for the inverse and thus the background term to be defined. Secondly, when solving the minimisation problem on a high reslution grid the dimensions of

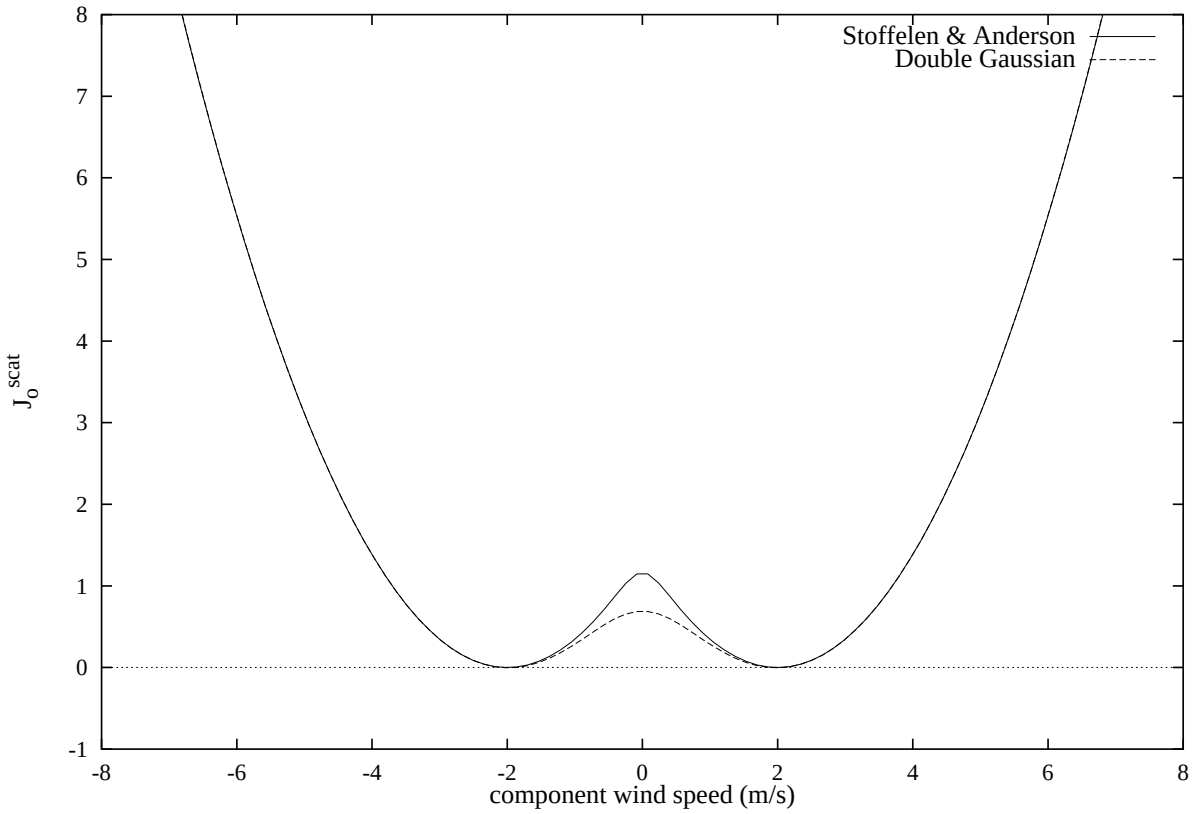

Figure 2.1: Cross-section along a component wind speed axis of the observational cost function for ERS scatterometers

$\mathbf{B}$ are very large making direct inversion very costly in terms of computing time and memory use. The problem is aggravated because during the minimization the cost function is evaluated numerous times.

To ensure that $\mathbf{B}$ is non-singular it must have non-zero Eigenvalues. This is the case if $\mathbf{B}$ is *symmetric* and *positive-definite*. From a meteorological point of view this structure for $\mathbf{B}$ can be obtained if the two-point wind error covariances are considered to be *homogeneous* and *isotropic*, i.e. a function of the separation distance. This assumption is frequently made when dealing with wind errors (Hollingsworth and Lönnberg [6]). The $\mathbf{B}$ matrix in this form can be reduced to a block diagonal matrix and indeed to diagonal form in spectral space. In diagonal form the inversion of $\mathbf{B}$ is trivial.

To show this mathematically we consider the background term

$$J_b = \delta\mathbf{x}^t\mathbf{B}^{-1}\delta\mathbf{x} \tag{2.10}$$

Let $\mathbf{i}$ and $\mathbf{j}$ be two points with a wind error defined at each point. Let $\mathbf{B_{i,j}}$ be a 2x2 wind error component matrix

$$\mathbf{B_{i,j}} = \begin{pmatrix} \mathbf{B}^{uu}_{\mathbf{i,j}} & \mathbf{B}^{uv}_{\mathbf{i,j}} \\ \mathbf{B}^{vu}_{\mathbf{i,j}} & \mathbf{B}^{vv}_{\mathbf{i,j}} \end{pmatrix} \tag{2.11}$$

or

$$\mathbf{B_{i,j}} = \begin{pmatrix} b^{uu}_{i_1,j_1} & b^{uv}_{i_1,j_1} & b^{uu}_{i_1,j_2} & b^{uv}_{i_1,j_2} \\ b^{vu}_{i_1,j_1} & b^{vv}_{i_1,j_1} & b^{vu}_{i_1,j_2} & b^{vv}_{i_1,j_2} \\ b^{uu}_{i_2,j_1} & b^{uv}_{i_2,j_1} & b^{uu}_{i_2,j_2} & b^{uv}_{i_2,j_2} \\ b^{vu}_{i_2,j_1} & b^{vv}_{i_2,j_1} & b^{vu}_{i_2,j_2} & b^{vv}_{i_2,j_2} \end{pmatrix} \tag{2.12}$$

The assumption of homogeneity makes $\mathbf{B}$ depend on the separation vector $\mathbf{i}-\mathbf{j}$.

$$\mathbf{B_{i,j}} = \mathbf{B_{i-j}} \tag{2.13}$$

The assumption of isotropy makes $\mathbf{B}$ depend on the separation distance $|\mathbf{i}-\mathbf{j}|$.

$$\mathbf{B_{i-j}} = \mathbf{B}_{|\mathbf{i-j}|} = \mathbf{B}_{|\mathbf{j-i}|} \tag{2.14}$$

hence $\mathbf{B}$ is symmetric. We follow Schyberg and Breivik [13] and introduce the variable

$$\delta\mathbf{z} = \begin{pmatrix} \mathbf{z}^u \\ \mathbf{z}^v \end{pmatrix} \tag{2.15}$$

so that

$$\delta\mathbf{x} = \mathbf{B}\delta\mathbf{z} = \sum_{\mathbf{i},\mathbf{j}} \mathbf{B}_{|\mathbf{i}-\mathbf{j}|}\delta\mathbf{z}_{\mathbf{j}} = \mathbf{B} * \delta\mathbf{z} \tag{2.16}$$

where the asterix denotes convolution. The assumptions of homogeneity and isotropy have converted the matrix vector product into a convolutional sum. The advantage of obtaining a convolutional sum is that convolution converts to ordinary multiplication under Fourier transform, which is computationally much more efficient. The discrete Fourier transform and its inverse are defined as

$$\delta\hat{x}_{\mathbf{k}} = \sum_{\mathbf{i}} \delta x_{\mathbf{i}} e^{-2\pi i \frac{\mathbf{k}}{\mathbf{n}}\cdot\mathbf{i}} \tag{2.17}$$

and

$$\delta x_{\mathbf{i}} = \frac{1}{N_1 N_2} \sum_{\mathbf{k}} \delta\hat{x}_{\mathbf{k}} e^{-2\pi i \frac{\mathbf{k}}{\mathbf{n}}\cdot\mathbf{i}} \tag{2.18}$$

respectively, with $\mathbf{n} = (N_1, N_2)$, $\mathbf{i} = (i_1, i_2)$ and $\mathbf{k} = (k_1, k_2)$ and

$$\begin{array}{rcl} i_1, k_1 & = & 0, ..., N_1 - 1 \\ i_2, k_2 & = & 0, ..., N_2 - 1 \end{array} \tag{2.19}$$

Using the convolution theorem of Fourier transform we obtain for (2.16)

$$\mathbf{B} * \delta\mathbf{z} = \hat{\mathbf{B}} \cdot \delta\hat{\mathbf{z}} \tag{2.20}$$

with

$$\hat{\mathbf{B}} = \begin{pmatrix} \hat{b}^{uu}_{0,0} & \hat{b}^{uv}_{0,0} & 0 & 0 & & & \cdots & \cdots & 0 & 0 \\ \hat{b}^{vu}_{0,0} & \hat{b}^{vv}_{0,0} & 0 & 0 & & & \cdots & \cdots & 0 & 0 \\ 0 & 0 & \ddots & \ddots & 0 & 0 & & & \vdots & \vdots \\ 0 & 0 & \ddots & \ddots & 0 & 0 & & & \vdots & \vdots \\ & & 0 & 0 & \hat{b}^{uu}_{k_1,k_2} & \hat{b}^{uv}_{k_1,k_2} & 0 & 0 & & \\ & & 0 & 0 & \hat{b}^{vu}_{k_1,k_2} & \hat{b}^{vv}_{k_1,k_2} & 0 & 0 & & \\ \vdots & \vdots & & & 0 & 0 & \ddots & \ddots & 0 & 0 \\ \vdots & \vdots & & & 0 & 0 & \ddots & \ddots & 0 & 0 \\ 0 & 0 & \cdots & \cdots & & & 0 & 0 & \hat{b}^{uu}_{N_1-1,N_2-1} & \hat{b}^{uv}_{N_1-1,N_2-1} \\ 0 & 0 & \cdots & \cdots & & & 0 & 0 & \hat{b}^{vu}_{N_1-1,N_2-1} & \hat{b}^{vv}_{N_1-1,N_2-1} \end{pmatrix} \tag{2.21}$$

The spectral form $\hat{\mathbf{B}}$ is a real-valued, symmmetric, block-diagonal matrix with a 2x2 block size. $\hat{\mathbf{B}}$ is of size $(N_1 \cdot N_2) \times (N_1 \cdot N_2)$ and can be made diagonal by means of a *unitary similarity transform*

$$\hat{\mathbf{B}} = \mathbf{R}\mathbf{\Lambda}\mathbf{R}^{-1} \tag{2.22}$$

Here $\mathbf{\Lambda}$ is the diagonal matrix of Eigenvalues which are real valued and positive. $\mathbf{R}$ is the transformation matrix of Eigenvectors. $\mathbf{R}$ is also block-diagonal and is unitary,

$$\mathbf{R}^* = \mathbf{R}^{-1} \tag{2.23}$$

The asterix superscript denotes conjugate transpose. With (2.10), (2.22) and (2.23) the background term of the cost function can be expressed as

$$J_b = \delta\mathbf{x}^{\mathbf{t}}\delta\mathbf{z} = \frac{1}{N_1 N_2}\delta\hat{\mathbf{x}}^*\delta\hat{\mathbf{z}} = \frac{1}{N_1 N_2}(\mathbf{R}^*\delta\hat{\mathbf{x}})^*\mathbf{\Lambda}^{-1}(\mathbf{R}^*\delta\hat{\mathbf{x}}) \tag{2.24}$$

where we apply the fact that the norm of a vector is preserved under Fourier transform. Now $\mathbf{R}$ represents a rotation in space of the frame of reference. As a result of this rotation we obtain

$$\hat{\mathbf{B}}_{\mathbf{k}} = \begin{pmatrix} \hat{b}^{uu}_{\mathbf{k}} & \hat{b}^{uv}_{\mathbf{k}} \\ \hat{b}^{vu}_{\mathbf{k}} & \hat{b}^{vv}_{\mathbf{k}} \end{pmatrix} = \begin{pmatrix} \hat{b}^{ll}_{\mathbf{k}} & \hat{b}^{lt}_{\mathbf{k}} \\ \hat{b}^{tl}_{\mathbf{k}} & \hat{b}^{tt}_{\mathbf{k}} \end{pmatrix} \tag{2.25}$$

The error covariances in $\mathbf{B}$ are now defined in terms of longitudinal and transverse wind components (see fig.A.1 in appendix A) where

$$\hat{b}^{lt}_{\mathbf{k}} = \hat{b}^{tl}_{\mathbf{k}} = 0 \tag{2.26}$$

so after the transform only the diagonal terms of $\mathbf{B}$ remain. The rotation implies for the block structure of $\mathbf{R}$ at each 2D wave number $\mathbf{k} = (k_1, k_2)$

$$\mathbf{R}_{\mathbf{k}} = \begin{pmatrix} \cos\theta & -\sin\theta \\ \sin\theta & \cos\theta \end{pmatrix} \tag{2.27}$$

with

$$\theta = \tan^{-1}\left(\frac{k_2}{k_1}\right) \tag{2.28}$$

If we denote for the diagonal matrix of equation (2.22)

$$\mathbf{\Lambda} = \sum_{\mathbf{k}} diag(\hat{b}^{ll}_{\mathbf{k}}, \hat{b}^{tt}_{\mathbf{k}}) \tag{2.29}$$

and define the spectral form of the longitudinal and transverse wind error components as

$$\begin{pmatrix} \hat{l} \\ \hat{t} \end{pmatrix}_{\mathbf{k}} = \mathbf{R}^*_{\mathbf{k}} \delta\hat{\mathbf{x}}_{\mathbf{k}} \tag{2.30}$$

We find for the background term

$$J_b = \frac{1}{N_1 N_2} \sum_{\mathbf{k}} \left(\frac{\left|\hat{l}_{\mathbf{k}}\right|^2}{\hat{b}^{ll}_{\mathbf{k}}} + \frac{\left|\hat{t}_{\mathbf{k}}\right|^2}{\hat{b}^{tt}_{\mathbf{k}}} \right) \tag{2.31}$$

In this form the computation of J_b can be carried out efficiently with a real to complex 2D FFT of the wind error component fields and the longitudinal and transverse covariance fields. The covariance fields are real and symmetric so their Fourier transforms are real. What remains is the exact specification of the longitudinal and transverse background error covariances as a function of distance.

2.4 The background error covariance matrix

Because of its size the background wind error covariance matrix **B** in 2D-VAR is not specified explicitly from the actual state of the atmosphere. For reasons of computational efficiency it is specified as a symmetric positive definite matrix. This structure of the matrix is obtained by applying the assumptions of homogeneity and isotropy, that make the covariances a function of distance only. To obtain a function of distance for background error covariances is a difficult but important problem. The structure of this function determines the spatial spreading of observational information in the analysis and so is a key feature in the performance of 2D-VAR.

Empirical covariance functions

Background wind error covariances are not directly observed. However with the assumptions of homogeneity and isotropy a statistical approach is possible based on observation-minus-background departures to obtain them. In meteorological practice this approach is known as the *observational method* and is credited to Hollingsworth and Lönnberg [6]. To assess the suitability of empirical covariance functions for 2D-VAR we applied the observational method to scatterometer observations and ECMWF winds as is explained in appendix A. The observational method generates error covariance functions based on mean covariances averaged over a longer period of time. This may result in error covariance functions that are less suitable in cases of extreme spatial variability for which scatterometer observations potentially have added value, and for which ambiguity removal is most

problematic. It is thus not a priori clear that this is an optimal method to achieve a good-working 2D-VAR.

2.5 Implementation of the scheme

2D-VAR starts by reading in a batch of ERS scatterometer messages, i.e. the location of the nodes in lat-lon and the ambiguous wind vector solutions. Also a 3 hour forecast for the 10 m wind is used. In the current regional implementation the forecast is obtained from the HIRLAM NWP model. The forecast corresponds to the observation time and is interpolated from the HIRLAM grid to the location of the scatterometer nodes. The interpolated forecast for the 10 m wind is subtracted from both wind vector solutions to yield observation increments.

To place the observations into the analysis grid the "centre of gravity" of all scatterometer nodes is computed. The centre of gravity provides the centre of the analysis grid. For each node in the scatterometer swath that contains a valid observation the grid cel location in the analysis grid and the nearest neighbour grid points are determined. The latter are needed to compute the interpolation weights used in the observation operator.

Observation grouping

In meteorological analysis of scatterometer data it is a problem to assimilate the smallest scales observed by the scatterometer. Typically the spatial width of structure functions is a few hundred kilometers. This does not allow analysis fits to the 50 km scale without serious overfitting effects. Traditionally this problem is solved by thinning the data to the 100 km scale (Stoffelen and Anderson [16]). Obviously thinning of data results in information loss and should be avoided if possible. Stoffelen and van Beukering [18] implemented averaging of scatterometer winds after AR with clear beneficial effect. However averaging of ambiguity removed winds is not an option in 2D-VAR. Averaging is also not simple to implement in 3D/4D-VAR without loss of information on wind solution ambiguity.

In 2D-VAR we apply observation grouping, i.e. the same location is assigned to a group of neighbouring scatterometer nodes. This has the effect of spatial smoothing of the scatterometer information and avoids introduction of statistical noise due to overfitting. In addition by merely reassigning location the information content of the scatterometer measurements is preserved. We therefore prefer observation grouping over thinning or wind-averaging.

The extended grid

The analysis grid of 2D-VAR is equidistant. The origin of the grid is defined in the lower left corner (fig.1.4). The dimensions of the grid are a power of 2 (64×64,128×128) which allows for efficient FFT. The grid spacing is flexible but nominally $1° \times 1°$.

The inner part of the grid is the bounding box around the scatterometer nodes. If the grid was only defined by this bounding box the situation may arise that background increments due to observations near the edge of the grid may result in large changes outside the analysis grid due to the spatial extent of the covariance function. For parts of the covariance function that fall outside the analysis grid no penalty would be defined for the background term. To avoid this from happening, the grid is extended outside the bounding box to incorporate an area that covers at least the region of influence of the structure functions when applied at the edges of the bounding box.

The use of this extended grid remedies a second complicating factor that concerns working in Fourier space. Applying Fourier transform requires the covariance and wind error component fields to be periodic to avoid Gibb's phenomenon and wrap-around effects. The extended grid described above makes sure that the covariance functions affect the edges of the extended grid only marginally. Also the first guess in the incremental formulation is periodic since it is zero everywhere.

Minimization

The analysis in 2D-VAR involves on the order of 10^4 grid points with 2 variables defined at each grid point. The selection of a suitable minimization algorithm for this type of large scale non-lineair minimization problem requires special care in matters concerning required storage, convergence and accuracy.

In meteorological practice two types of minimization methods are mostly used for large scale variational analysis. *Conjugate gradient* (CG) and *quasi-Newton* (QN) methods. Both methods are iterative and suited for unconstrained minimization of non-lineair objective functions. The CG method has favourable storage requirements compared to QN methods. For the minimization of a problem with N variables on a discrete grid they require storage of only a few vectors of size N. Quasi-Newton methods on the other hand require the storage of a Hessian matrix of size NxN which makes them rather unsuitable for 2D-VAR. They do have better convergence rates than CG-methods however. In addition, variable storage quasi-Newton methods

have been developed (Gilbert & LeMarechal [5]) and applied succesfully in variational data assimilation (Courtier [19]). For 2D-VAR the Polak-Ribiére form of the conjugate-gradient method by Press [11] was selected because of its availability as off-the-shelf routine. For an in depth discussion on the minimization methods mentioned and their application in meteorology see Navon and Legler [9].

The optimal solution of the minimisation problem is found by solving the gradient equation

$$\nabla J(\delta \mathbf{x}) = 0 \tag{2.32}$$

The CG-method requires the evaluation of the gradient of the cost function. For the background term the gradient in spectral space is (see (2.24))

$$\nabla_{\delta \hat{\mathbf{x}}} \hat{J}_b = 2(\mathbf{R}^*)^* \Lambda^{-1} (\mathbf{R}^* \delta \hat{\mathbf{x}}) \tag{2.33}$$

The gradient on the analysis grid is then obtained by an inverse Fourier transform. The expression for the gradient of the observational term is rather lengthy and is not mentioned here. Its derivation however is straightforward from equation 2.8. The minimization process starts with the null vector as first guess for the state vector of wind increments. The minimization stops if the difference in cost function value between two consecutive iterations is smaller than a specified number or if a maximum number of iterations has been carried out, in which case 2D-VAR has failed to converge and no solution is presented.

Chapter 3

Experiments and Results

Empirical covariance functions

To compute background error covariances we used scatterometer data from ERS-2 for latitudes between 30N and 90N. The scatterometer winds were from the month of September 1995 and February and March of 1996. The ambiguity in the scatterometer data was removed using the PRESCAT method. The background winds were 3-9h forecasts for the 10 m wind from the ECMWF T213 global NWP model. The background winds were interpolated in space and time to the observation points.

The winds were split into their components and the background winds were subtracted from the scatterometer winds to obtain the observation-minus-background component departures. The departures were corrected for a small deviation from zero in the mean as can be seen from figure 3.1. The figure shows that the bias in the wind component departures is very small in the range of -15 m/s to 15 m/s. The bias in the mean is -0.03 and -0.08 m/s for the u and v component departures respectively.

Next the wind departures were organised in grid boxes and averaged so that the resolution of the data corresponds to the analysis grid in 2D-VAR. The longitudinal and transverse component departure covariances l and t were computed according to the procedure described in Appendix B. In order to compute covariances over sufficiently long distances the scatterometer messages were grouped into batches of adjacent messages. Next a histogram of departure covariances was computed as a function of separation distance between observations for all combinations of observation pairs in the along-track direction. The departure covariances are composited in bins and averaged.

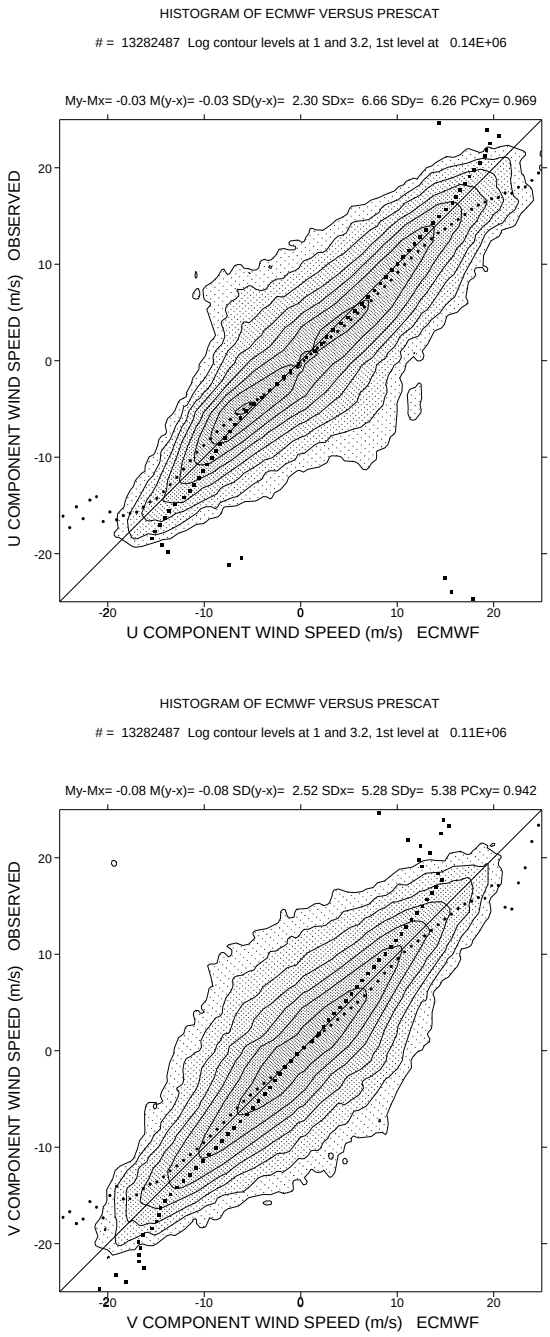

Figure 3.1: Statistical properties of the u and v component departures for the ERS-2 dataset of 09/95 and 02-03/96.

Figure 3.2 shows the mean background vector and component error covariances as function of distance using a 100 km bin size. A Fourier-Bessel function is fitted through the error covariances. The rationale for using this function is explained in appendix A.

As can be seen in panels A, B and C of figure 3.2, the mean error covariances go to zero asymptotically at large distances. This made us decide to use the zeros of J_1 in the Fourier-Bessel series indicating a zero gradient as boundary condition. We used 5 terms in the model functions and the value r_0 (see appendix A)was selected at 1350 km.

The model functions for the longitudinal and the transverse wind error component covariances (panel A and B) were obtained by a simultaneous fit with the constraint of equal zero intercept due to the isotropy assumption. The background component variance turns out to be 2.63 m^2/s^2. The transverse component covariances decrease slightly faster than the longitudinal ones. It does not exhibit a negative lobe which is typical for winds above the boundary layer. Such a negative lobe results when computing covariances in the upper troposphere (Hollingsworth and Lönnberg [6]). Finally in figure 3.2, panel C shows that the background wind error variance is 5.26 m/s whereas the total wind error variance is 11.7 m/s, i.e. background winds are slightly more accurate than scatterometer winds, consistent with Stoffelen [14]. Also the results fall within the ensemble of curves obtained by Homleid [7].

Figure 3.3 shows the spectra of the Fourier-Bessel function of the longitudinal and transverse component covariance function as well as the wind error vector covariance function. The spectra are positive definite so they can be applied in 2D-VAR.

In figure 3.4 a 2D footprint of the wind error component covariance functions is shown. From this figure it is evident that the component covariance functions exhibit only weak rotational features. The lack of rotation is probably due to friction near the Earth's surface. It is questionable whether these empirical covariance functions are suitable for extreme atmospheric conditions involving small scale vortices. In general the drawback of using average covariances is that they may not be representative for the wind error structure of the atmosphere in an individual case, or, more in particular, of the wind error structure in cases of problematic ambiguity removal.

As can be inferred from figure 3.2, the mean error covariances have sharp peaks at short distances. This becomes more apparant if a 50 km bin size is used. An attempt

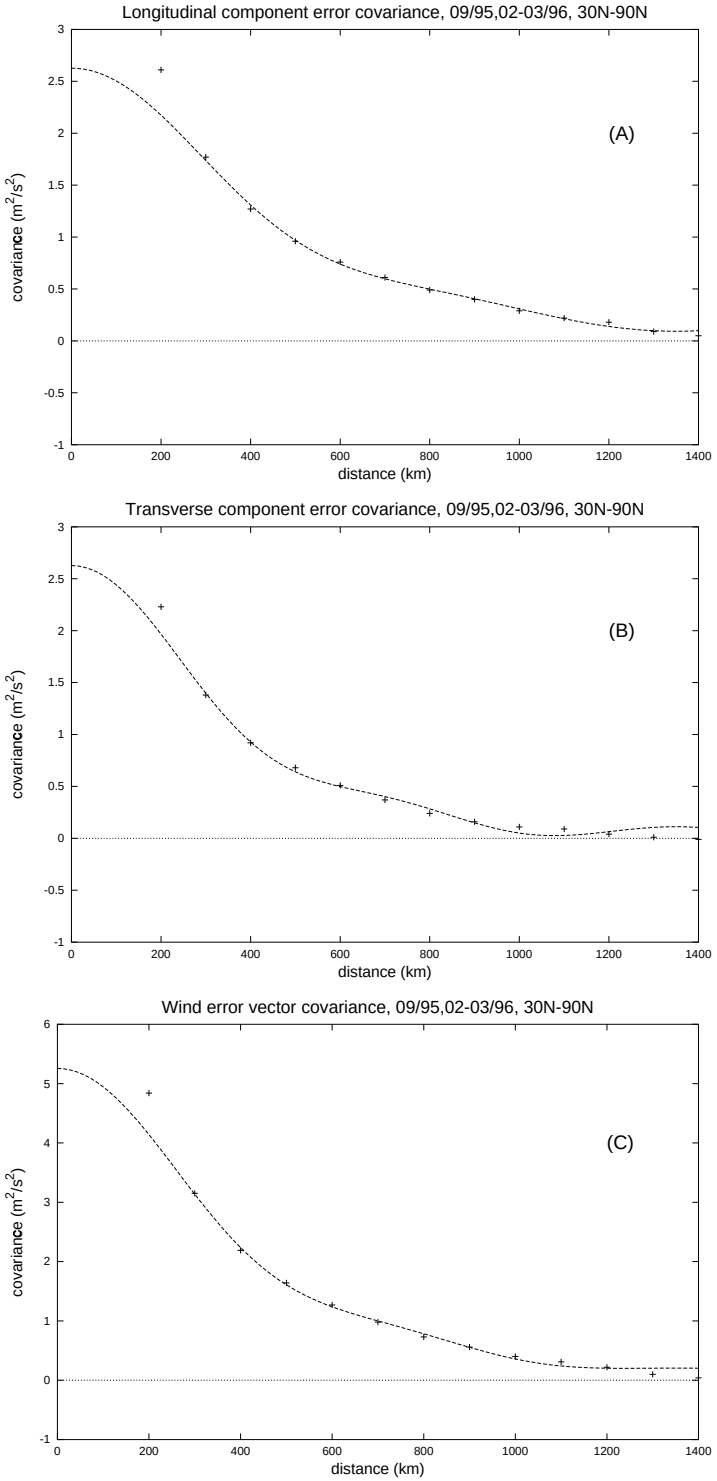

Figure 3.2: Empirical error covariance functions.

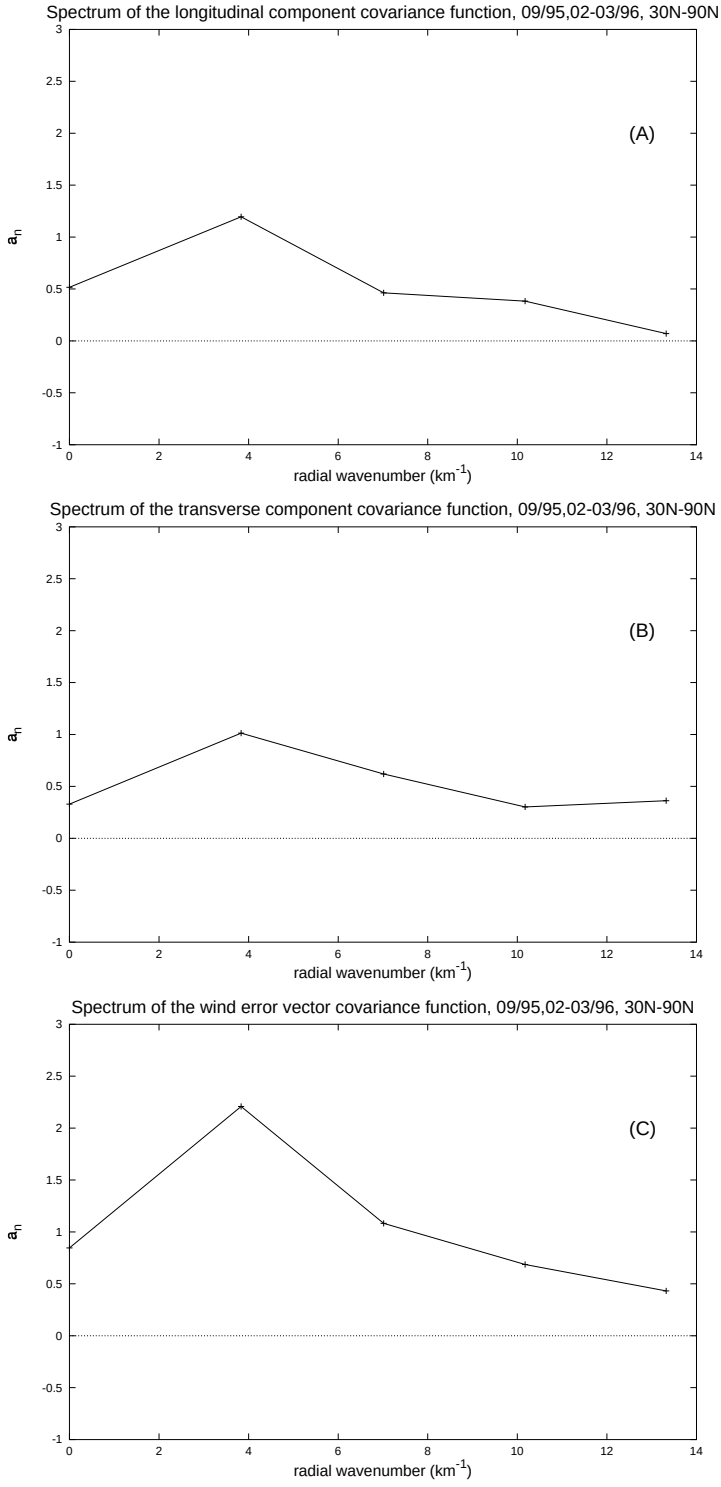

Figure 3.3: Empirical error covariance spectra.

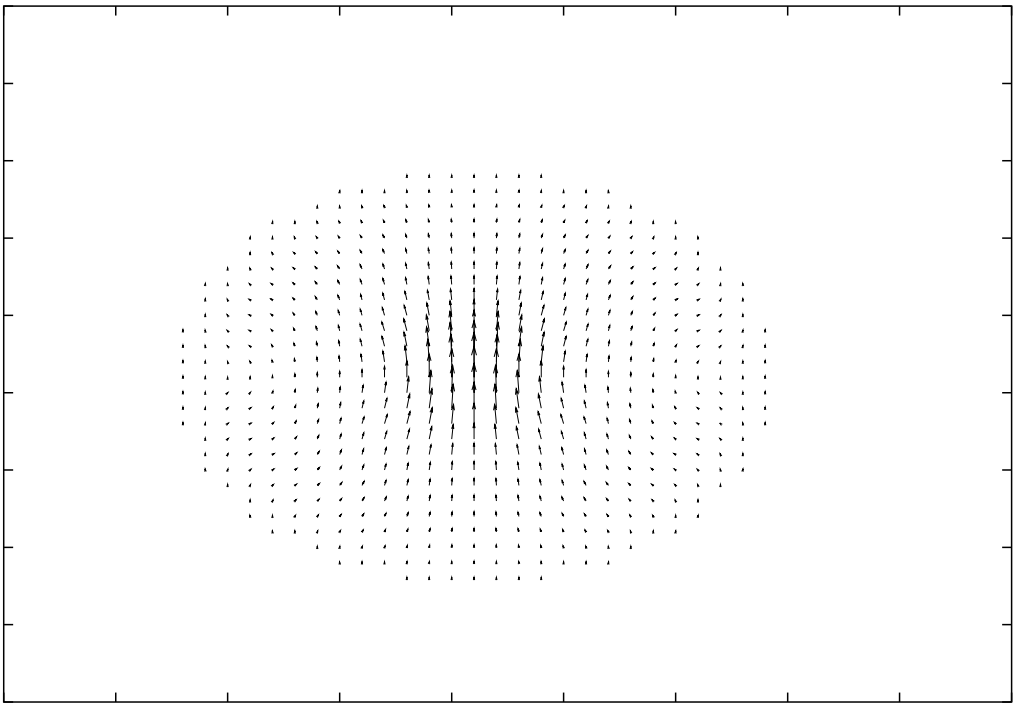

Figure 3.4: Vector plot of the 2D footprint composed of the empirical error component covariance functions for the longitudinal and transverse components.

to fit the model function with more terms at 50 km results in error covariance functions that exhibit ondulations and spectra that are not strictly positive-definite, i.e. they show serious signs of overfitting. This has kept us from running 2D-VAR at 50 km resolution.

A single observation experiment

As a system test we consider the case of one observation. This should verify if 2D-VAR is able to spatially spread the observational information. Figure 3.5 illustrates the result when 2D-VAR is presented with a wind vector of 25 m/s that is directed to the North. The reponse shows the footprint of the structure function on the analysis grid. An unresolved peculiarity is that it shows less rotation than the footprint in fig 3.4 which it should resemble.

3.1 Case studies

It is important to know the behaviour of 2D-VAR in difficult situations. The strength and weaknesses of 2D-VAR have been studied for a number of meteorologically relevant conditions for the near-surface wind. Cases were analysed after monitoring the difference in wind vector selection between 2D-VAR and PRESCAT. In all following cases 2D-VAR was run on a 64×64 analysis grid using the empirical covariance functions of figure 3.2. The background wind is a 3 hour forecast from HIRLAM for the 10 m wind, corresponding to the observation time and interpolated to the scatterometer nodes. Observation grouping is applied with a 100 km spacing in the observational data unless stated otherwise.

Absence of a low-pressure system in the background wind field

Figure 3.6 shows a situation where the scatterometer has observed a strong cyclonic flow that is non-existent in the background wind field. The upper left panel shows the PRESCAT solution for this case. It clearly shows the vortex but appears unmeteorlogical on the upper right side of the low pressure center. The upper left panel shows the background wind, a 3 hour forecast for the 10m wind. The background wind does not show any small-scale vortex. The surface wind in the lower left panel, (background wind plus 2D-VAR analysis increments) gives a smooth and consistent wind field with the vortex at the location depicted by the scatterometer data (panel A). In the 2D-VAR wind vector product which is based on the analysis result (lower right panel) the inconsistency of PRESCAT is no longer present. The 2D-VAR product is more realistic and is arguably better than PRESCAT.

Figure 3.5: The error covariance function footprint on the analysis grid.

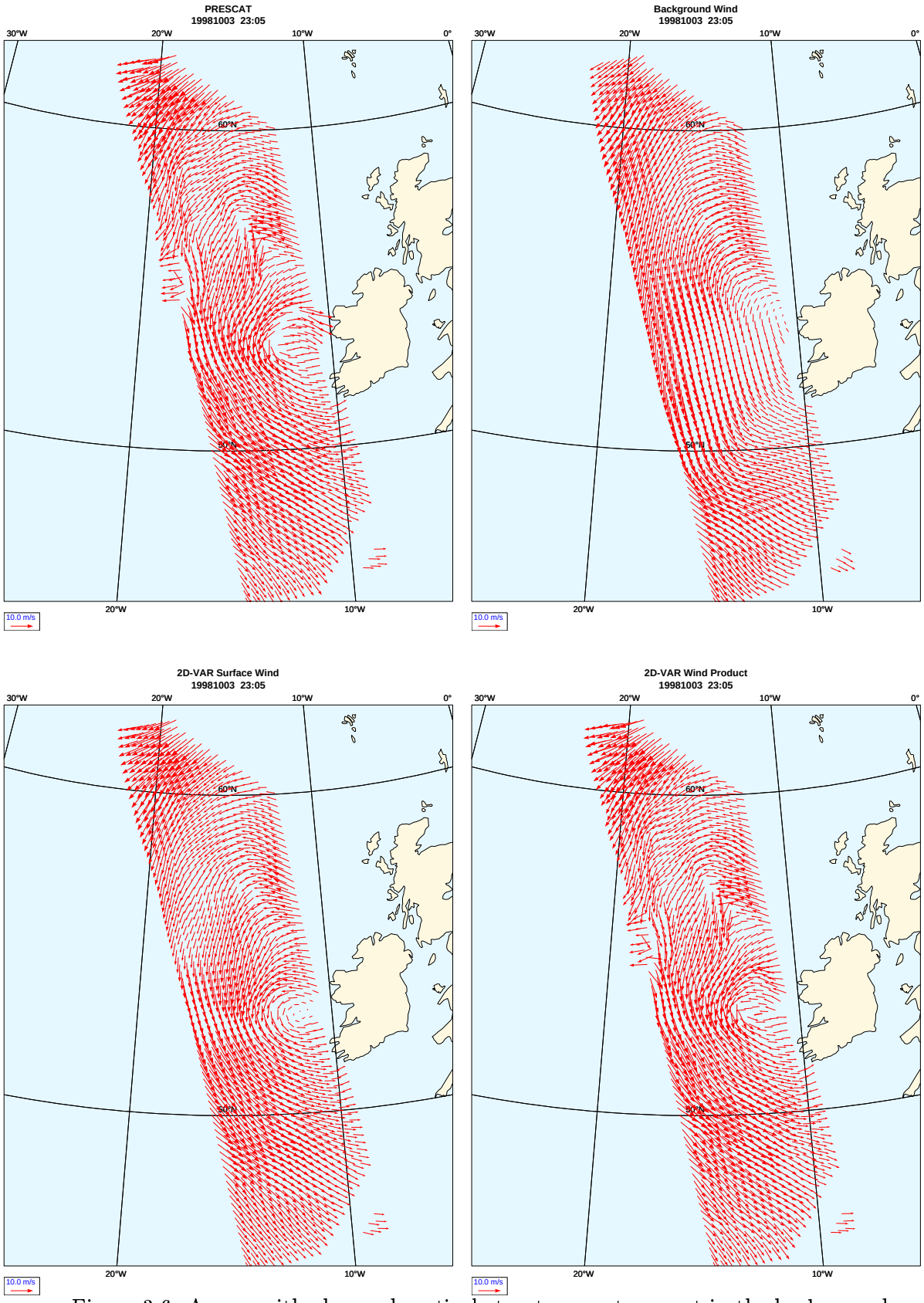

Figure 3.6: A case with observed vortical structures not present in the background field.

The effect of observation grouping

To show the effect of observation grouping we consider a case on the scatterometer swath with a wind field that has a sharp frontal zone. Figure 3.7 shows the PRESCAT solution (upper left panel) on the swath. PRESCAT is able to delineate the front very sharply. The background field (upper right panel) also has a well defined front but its exact position is a little more to the North in the lower left part of the swath. The direction of the wind in the background field starts to deviate along the front towards the lower left part of the swath compared to the wind direction in the observations. Because of this 2D-VAR analysis without observation grouping creates a small vortical structure in the surface wind (lower left panel). The 2D-VAR analysis is able to bring the wind direction near the front more in line with the observations but it maintains the difference in the exact position of the front that is already present in the background field. This phase difference is also found in the 2D-VAR wind product resulting in an area on the lower left part of the swath with a somewhat erratic character. The PRESCAT product is therefore more consistent in this case.

Figure 3.8 shows the same case but with observation grouping applied in 2D-VAR (resolution 100 km). In this case the vortical structure of figure 3.7 is absent in the surface wind based on the 2D-VAR analysis (lower left panel). As a result the size of the area that exhibits the erratic character in the wind field has diminished in the 2D-VAR wind product. Also the difference in the position of the front seems to have changed a little and is closer to that in PRESCAT. The 2D-VAR wind product has improved somewhat but PRESCAT is still more consistent.

A mispositioned low pressure system

In the upper panels of figure 3.9 a situation is depicted on the scatterometer swath where a small-scale low pressure system is mispositioned in the background field compared to that in the observed winds. The correct solution in this case would show a small-scale vortex in the middle of the swath at the lower edge of the panel. The PRESCAT solution neutralizes the vortex at its position in the background field but is not fully capable of producing the vortex in the middle of the swath at the lower part of the panel. It produces an area to the right of the shear line where the wind direction is probably wrong.

The surface wind based on the 2D-VAR analysis (lower left panel) shows a weaker, stretched vortex about halfway between the position it has in the background field and in the observations. The 2D-VAR wind product gives a result similar to

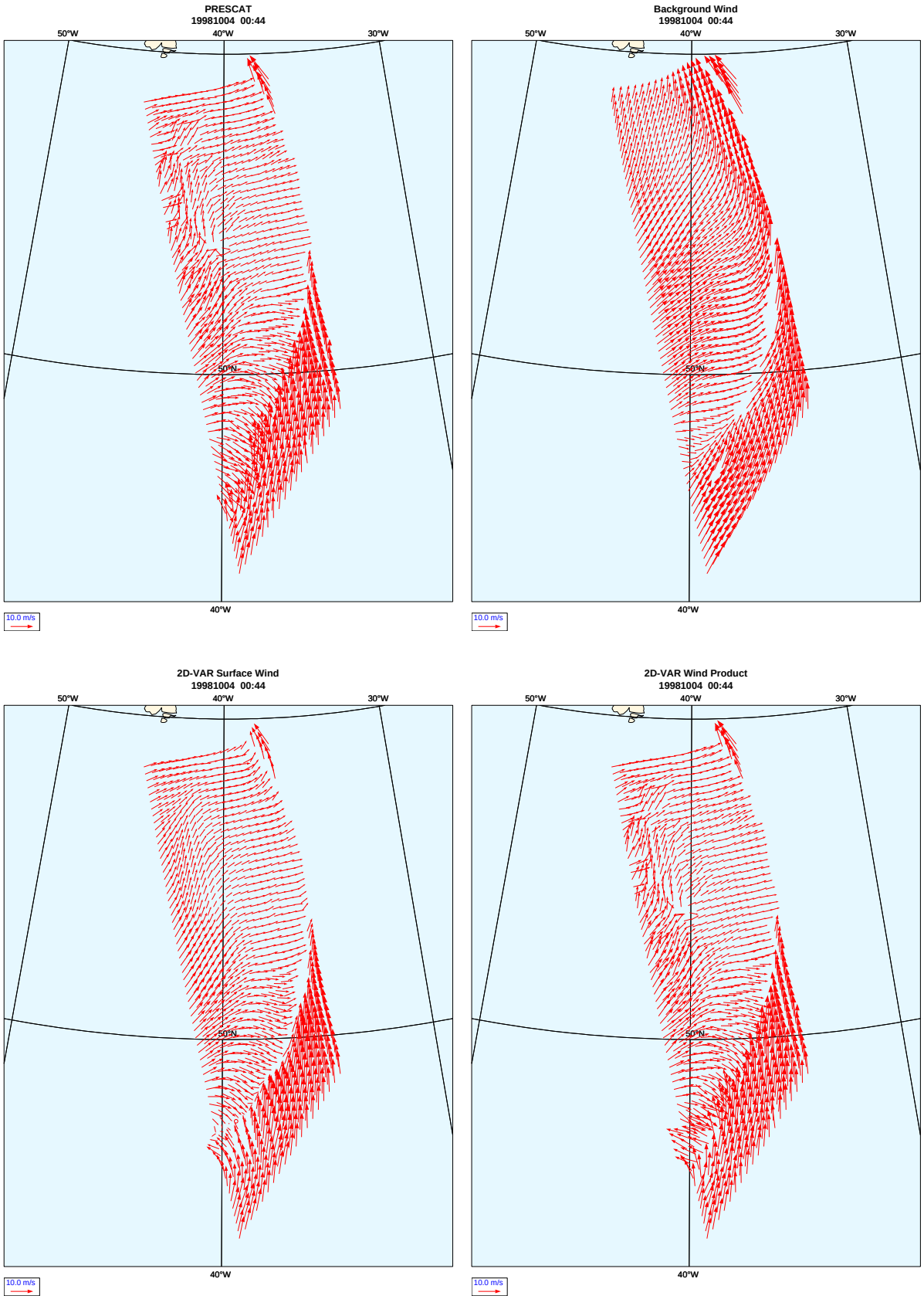

Figure 3.7: Case without observation grouping in 2D-VAR for a wind field with a frontal zone.

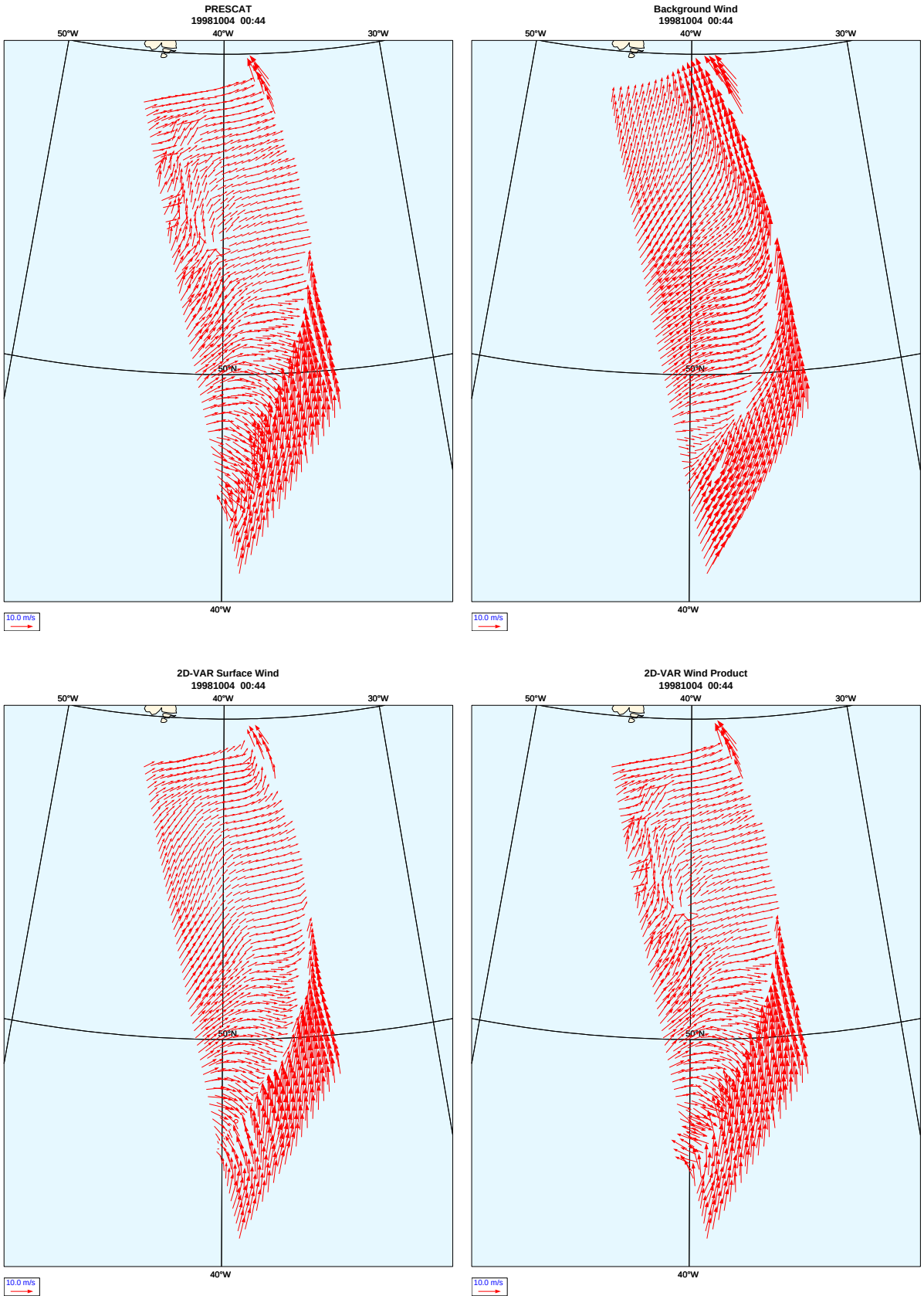

Figure 3.8: Case with observation grouping in 2D-VAR for a wind field with a frontal zone.

PRESCAT but the shear line is in a different position. The area of wind with a wrong direction is larger. The 2D-VAR wind product offers no real improvement over PRESCAT. Comparing fig 3.9 with figure 3.6 shows a similar system differing mainly in size. This gives rise to the notion that succesful ambiguity removal depends on the scale of weather systems in relation to the shape and spatial extent of the covariance functions, i.e. the background error structures are situation-dependent.

We have tried to find out if changes in characteristic length scale would improve the solution in the above individual cases. Therefore we used quasi-geostrophic covariance functions which are parametric (see appendix C). The results were similar to that with empirical covariance functions but on average gave no real improvements. The so-called situation-dependency of covariance function will require further investigation.

3.2 Objective Validation of 2D-VAR

To assess whether 2D-VAR represents an improvement in ambiguity removal skill, an automated comparison study was carried out. The 2D-VAR and PRESCAT scheme were used to remove the ambiguity in the wind vector solution of ERS-2 data in the HIRLAM model area for the period of May 20th to May 26th 1999. The solution for the near-surface wind field from both schemes was compared with the HIRLAM analysis for the 10 m wind closest to the observation time. This analysis, interpolated to the scatterometer nodes, is itself not based on scatterometer observations and is assumed to be the most accurate estimate of the near-surface wind field known at that particular time. The wind vector difference between the result of either scheme and the analysis was computed and composited in a scatter plot.

To enhance the ability to determine the quality of the results both PRESCAT and 2D-VAR used a relatively poor quality 24 hour HIRLAM forecast for the 10m wind as background instead of a 3 hour forecast(see also Schyberg and Breivik [13]). The reason for this is that the analysis is less correlated to a 24 hour forecast than to a 3 hour forecast, which makes the verification more meaningfull. 2D-VAR was run on a $1^\circ \times 1^\circ$ grid of 64×64 nodes. In 2D-VAR the scatterometer observations were grouped with a 100 km spacing. The validation was carried out using the empirical error covariance functions of figure 3.2.

Figure 3.10 shows that in cases where PRESCAT and 2D-VAR have made a different selection for the wind vector solution, 2D-VAR has a larger RMS wind vector difference with the HIRLAM analysis in 55% of cases.

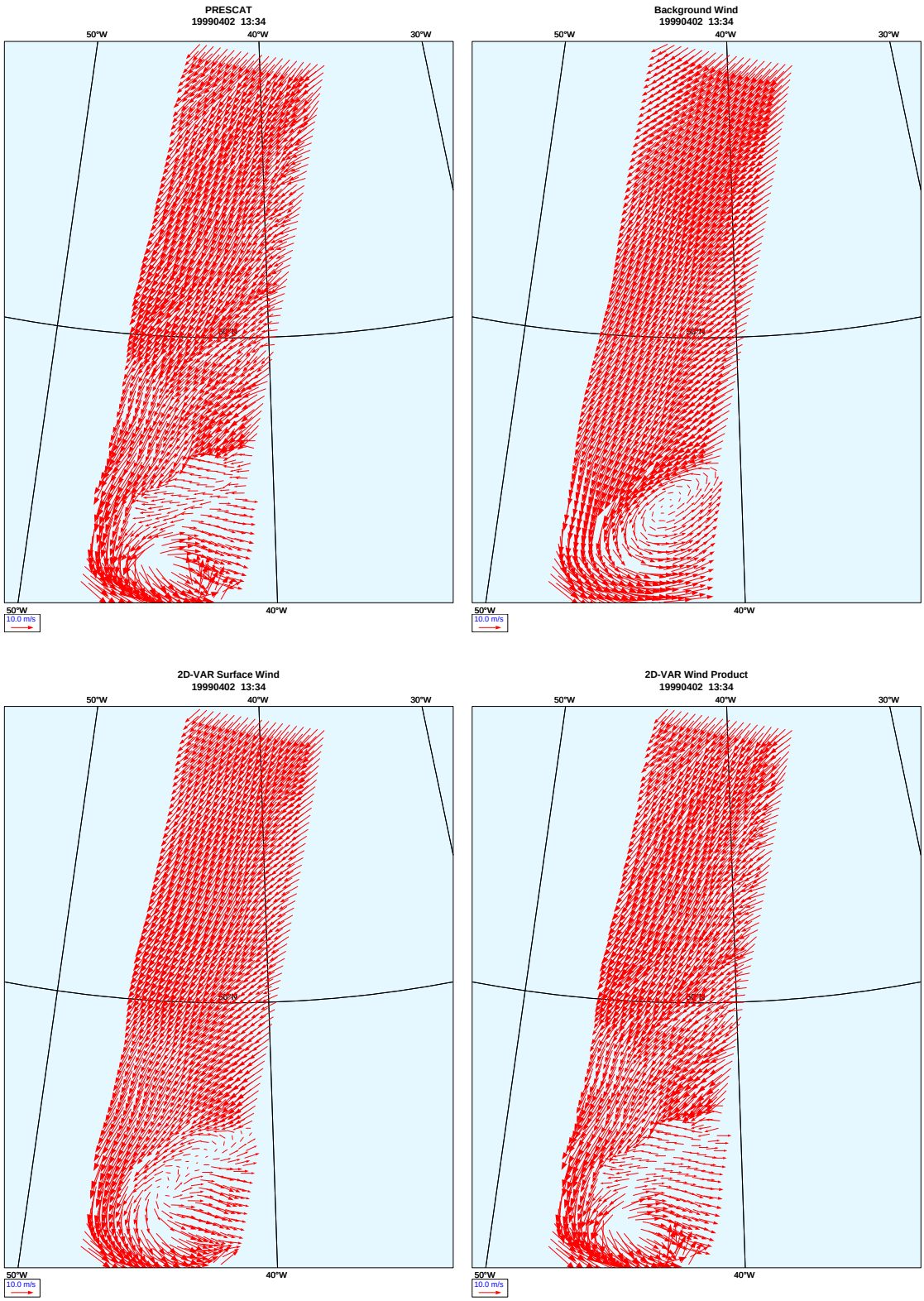

Figure 3.9: Case with a different position of a low pressure system for the background field compared to the observations.

Remark: Although this test is probably as objective as can be, there is a drawback. HIRLAM analyses do not contain the small-scale information present in scatterometer observations. In cases where small-scale features are present in the observations, the analyses do not contain any appropriate referential information. What is tested then is a mismatch with larger scale information that makes a comparison incomplete. Thus the results of the test are only indicative and may not give a clear picture on the relative performance of 2D-VAR.

Apart from the remark given above which is hard to verify, it must be noted that the test was run only over a short period.

3.3 Subjective Analysis

The objective test of the previous section has its limitations to validate the performance of 2D-VAR. To overcome the problem of the objective test a subjective analysis was carried out by meteorologists at KNMI. The human skill to recognise small-scale patterns is much better than that of any computer. In addition the meteorologists have some independent data sources that they can use for validation purposes. Moreover with their knowledge of atmosphere dynamics they can make a good analysis of meteorological conditions and so decide which solution for the near-surface wind field (2D-VAR or PRESCAT) is best in a given situation.

The meteorologists were asked to compare two wind products based on ERS scatterometer observations. The wind products were different only in the way in which ambiguity removal was carried out (2D-VAR vs. PRESCAT). Wind products were available for the North Atlantic region. The validation started in October/November of 1999. Due to some start up problems validation work was carried out routinely since the beginning of december 1999. It turned out that extra time was needed to

- inform meteorologists on the interpretation of the wind product
- incorporate validation activities in the work schedule of the meteorologists
- implement an effective way to record results.
- suit the presentation of the wind products to the meteorologist

The validation ended on February 1st 2000.

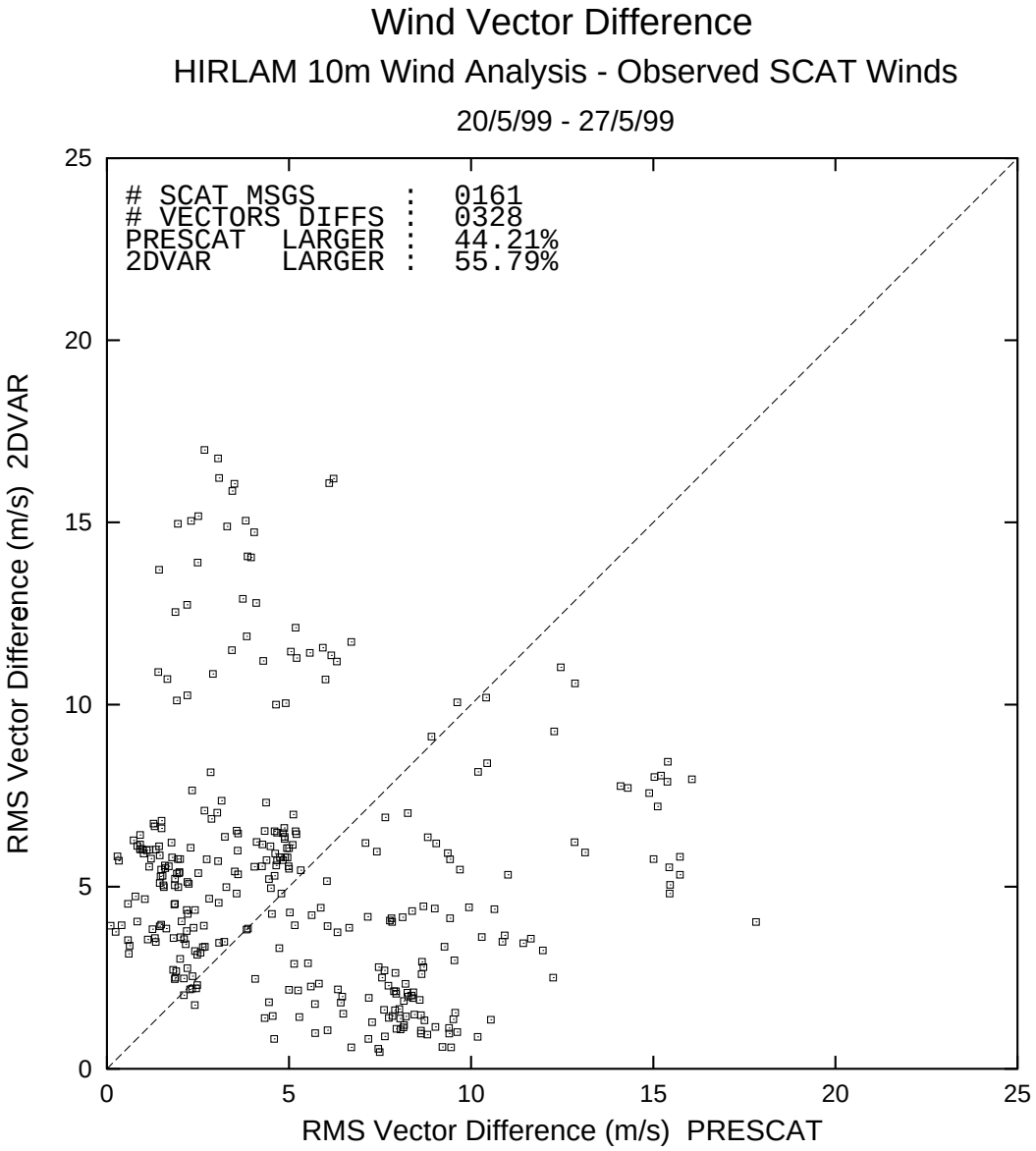

Figure 3.10: Scatterplot of the RMS wind vector difference between HIRLAM 10 m wind analyses and PRESCAT/2D-VAR.

The validation procedure

In the validation period the meteorologist during his/her shift was notified by e-mail when significant differences were present between the wind products pertaining to ambiguity removal, i.e. the wind vector difference over 361 nodes should be larger than 100 m/s. The wind products with differences were available on the KNMI Intranet. The meteorologist was asked to classify and judge the wind products after an analysis of the local atmospheric conditions at the observation time. Next the meteorologist was asked about the usefulness of the products in the situation at hand. Finally he/she was asked to write down the findings and additional remarks on a form (see figure 3.11) and put the form in a map for storage.

Results

For the validation forms of the period December 22 1999 to January 31 2000 were considered. The information in the forms was compiled into tables (see tables 3.2, 3.3 and 3.4, in Dutch !). The findings do not constitute a homogeneous series. This was due to

- the fact that the validation work could not be continued during weekends
- problems with a change in the BUFR messages for the ERS scatterometer observations in the period of January 17 to January 21 2000
- the fact that cases with significant differences did not occur every day
- sometimes the meteorological data needed to analyse atmospheric conditions was no longer available at evaluation time

To get insight in the data, the information on classification and judgement were extracted from the tables and put into a score matrix (see table 3.1). Scores ending on .5 result from assigning a particular case to two classes by the meteorologist. The score matrix shows that 2D-VAR ambiguity removal is better than PRESCAT for developing/decaying weather systems (classification 1, judgement 2), see for example figure 3.13, and for developed systems with sharp gradients (2,2). On the other hand PRESCAT is better in situations with sharp fronts, troughs and ridges (3,1), see for instance figure 3.14.

From the score matrix it also follows that in a large number of cases no appreciable differences between the wind products were determined (1-3,3). In the tables 3.2-4 we see that part of the reason for this, meteorologists argued, was that the meteorological conditions were very complex for those cases. In many cases with judgement

Judgement	Classification				Total
better:	1[a]	2[b]	3[c]	4[d]	
1 Prescat	4	2.5	8.5	3	18 (25%)
2 2D-VAR	9.5	4	6.5	8	28 (38%)
3 neither	10.5	6.5	8	2	27 (37%)

[a]developing or decaying weather system, saddle area
[b]developed system with sharp pressure gradient(s)
[c]sharp front, ridge or trough
[d]different, namely...

Table 3.1: Score matrix for the subjective analysis in PRESCAT/2D-VAR validation

3 a majority of meteorologists remarked that the wind products did not have added value. This opinion appeares to be due to the fact that the character and/or the location of weather systems in the wind products were not relevant for operational use. On the other hand some situations (see figure 3.15) were not interesting at all. Selection of these cases could probably have been avoided with a higher threshold for 'significantly different' cases. Finally the scores for classification 4 were mostly stationary areas of high pressure.

Usefulness of the wind products

In the tables we can see that the meteorologists use either wind product to extract additional information on the location, structure and intensity of weather systems, i.e. fronts, troughs, ridges, saddle areas and depression nuclei. Notably in data-poor areas the wind products are a useful addition to what they already have. The wind products are noted as useful analysis tool for national weather services (see for example figure 3.12 and figure 3.13).

In the figures the PRESCAT wind product is in the left panel and the 2D-VAR wind product is in the right panel. The background in both wind products is an infrared METEOSAT image, taken within a 1.5 hour time interval around the time of observation of the scatterometer winds. The filled blue areas over sea have an SST lower than zero. In these areas scatterometer wind observations are ussually not useful. The sky blue and purple arrows are 3 hour HIRLAM 10 m forecast winds. The red arrows are scatterometer winds. In the 2D-VAR wind product of figure 3.12 and 3.14 the PRESCAT solutions are represented as green arrows to mark the differences.

Beoordelingsformulier verschillen Prescat en 2D-VAR

S.v.p. (tenminste) één formulier per bericht:

DTG:

Message nr.:

Meteoroloog:

A. Classificatie

Zou je deze situatie kenmerken als (omcirkelen s.v.p.):

1. **ontwikkelend of opvullend systeem, zadelvlak,**
2. **ontwikkeld systeem met sterke drukgradient,**
3. **scherp front, rug, of trog, of**
4. **anders, namelijk:**

B. Beoordeling

Is in dit geval (omcirkelen s.v.p):

1. **Prescat beter,**
2. **2D-VAR beter,**
3. **is er geen substantieel verschil.**

C. Wat kun je er mee doen ?

Zijn beide oplossingen (Prescat en 2D-VAR) even waardevol voor de meteorologische analyse of is er een verschil in bruikbaarheid?

1. **Hoe zou je het kunnen gebruiken?**

2. **Is er een verschil in het gebruik van Prescat en 2D-VAR in dit geval?**

D. Eventuele opmerkingen:

Bedankt voor de medewerking!

Figure 3.11: Question form for findings of subjective analysis.

DTG	MSG NR	MET	Class.	Beoord.	Nut		Opmerking(en)
					hoe te gebruiken	verschil in gebruik	
1999122215	03	Drp	2	3	Detail structuur	-	53N41W 2D-VAR beter 53N43W geen uitsluitsel, wellicht beide fout
1999122312	22	Ltk	2	3	Positiebepaling depressiekernen	nee	
1999122321	10	Ltk	1	2	Vaststellen as zadelgebied	Nee, hoewel PRESCAT lijkt fout	
1999122400	05	Ltk	2	3	Bepaling intensiteit depressie (kerndruk,wind)	Nee	Interessant gebied!
1999122400	19	Ltk	1	2	Prescat geeft verwarrende 'foute' info	Ja, Prescat niet te gebruiken	
1999122312	13	Ltk	1	3	Geen relevante aanvullende informatie	Nee	
1999122312	05	Ltk	1	1	Vrijwel geen verschil	Vrijwel niet	Beide oplossingen leveren veel meer detail dan meteorologische analyse
1999122615	06	Plp	1	3	Weinig verschil	Alleen lage windsnelheden	
1999122812	13	Ntt	1	3	Weinig extra info		Er waren verschillen tussen Prescat en 2D-Var maar die bevonden zich niet in het zadelgebied
1999122812	17	Ntt	4	3	Weinig zinvol midden in hogedrukgebied		Situatie midden in omvangrijk hogedrukgebied Er waren verschillen maar gezien de lage windsnelheden geen keuze in beoordeling
1999122900	04	Ntt	2,3 trog	1			2D-VAR laat een klein gebiedtje met onwaarschijnlijke windsnelheden zien
1999122912	05	Vrg	1	2	Prescat geeft 'foute' informatie	2D-VAR gebruiken, windsnelheden echter te fors	Langzaam opvullend laag, zwakke drukgradient 72N04W
1999122912	20	Vrg	3	2	Levert meer detail dan HIRLAM analyse		Scherp front ter hoogte van 65N30W trog ter hoogte van 65N33W
1999122915	07	Vrg	3,rug	1			
1999122921	12	Vrg	4	2		Windsnelheden zijn gering	
1999123012	15	Mlk	1	2	Waarnemingen en vooral satelliet image suggereren zwakke cyclonale ontwikkeling	2D-Var bevestigt Class. -1-	2D-Var beter in zuiden
1999123015	03	Mlk	1,2	3	In gebied met sterke winden, beter beeld van windveld rond diepe stormdepressie	neen	Classificatie 1: tegen de Groenlandse kust Classificatie 2: in zuiden
1999123100	09	Mlk	3,front	1	Prescat: Positie van het koufront en sterke windruiming achter front beter te analyseren	Ja, 2D-VAR heeft wind achter koufront 180 grd gedraaid (misleidt?)	Prescat wordt bevestigd door SHIP
1999123103	06	Mlk	1	2	Positie (baan) depressiekern	Prescat winden 180 grd gedraaid. (Misleidt?)	2D-VAR beter in het zuiden, aan noordflank depressie
1999123103	09	Mlk	2	2	Analyse restlaag voor Groenlandse kust beter door 2D-VAR	Ja, Prescat 180 grd gedraaid.	
2000010300	12	Grn	1,3 trog	2	Ligging front		
2000010300	06	Grn	4	2	zwakke winden, meteorologisch niet relevant, wind wordt bepaald door sterke druktendens en niet door gradient		zwakke rug van hoge druk, wind wordt isallobarisch bepaald door drukdaling door stormdepressie tussen IJsland en Schotland
2000010312	08	Htk	1	3	Geven geen duidelijk andere informatie	Nee	beide oplossingen mogelijk ; zadelgebied
2000010312	16	Htk	1	1	Blijft ?	Nee	
2000010315	07	Htk	2	1	?	Nee	
2000010400	07	Htk	1	3	?	Nee	
2000010400	06	Htk	4	2	?	Nee	Situatie: dichtbij de kern v.e. laag
2000010400	11	Htk	1	3	?	Nee	
2000010400	14	Htk	1	2	?	Nee	
2000010412	13	Drp	3,front	3	Stromingspatroon complex, onvoldoende SFC obs. voor beoordeling. Noordzijde front Prescat beter, zuidkant 2D-VAR. Ze kunnen daar ook beide fout zijn	-	
2000010415	01	Drp	2	2	Prescat verwerpen	Prescat levert geheel 'foute' waarnemingen die tegen de sterke drukgardient in staan	
2000010500	01	Drp	4	2	Prescat niet te gebruiken wind waait tegen grad. in		

Table 3.2: Findings of the meteorologists

DTG	MSG NR	MET	Class.	Beoord.	Nut		Opmerking(en)
					hoe te gebruiken	verschil in gebruik	
2000010500	01	Drp	4	2	Prescat niet te gebruiken wind waait tegen grad. in		
2000010500	06	Drp	1	1	Geen waarnemingen beschikbaar Keuze Prescat op v. basis HIRLAM 21+03 Beter te positioneren as zadelgebied		Situatie: zadelvlak
2000010500	12	Drp	4	2	Prescat levert foute waarneming en is in dit gebied onbruikbaar		Situatie: vlakke hogedruk uitloper
2000010512	12	Slk	3	3	Analysetool voor IJsland/UK-met	Nee	
2000010621	08	Vrg	3	2		-	Situatie: trog, zeer zwakke gradiet
2000010621	13	Vrg	2	2		Prescat levert onjuiste info, 21 UTC waarnemingen sporen met 2D-VAR	
2000010700	07	Vrg	2	3	Positiebepaling centrum lage drukgebied		
2000010700	16	Slk	2	1	Trogas scherper leggen	gering	
2000010900	11	Slk	3	2	Trog/rug nauwkeuriger leggen	Ja, Prescat vectoren 2π gedraaid	
2000010900	16	Slk	3	2	Correcte katabatische winden vanaf Groenland plateau	Ja, Prescat laat de wind 2π tegen 't massief ingegaan	
2000010915	10	Grn	4	1	Positie frontale vore		Situatie: hogedrukgebied door een zwakke front. vore Beoordeling: Prescat beter op basis van SHIPS
2000010921	01	Grn	4	3		Geen significante bijdrage te weinig gradient	Situatie: stationaire drukverdeling tussen hoog NW en laag oost
2000011000	01	Grn	4	1		Geen toegevoegde waarde vanwege zwakke winden	Situatie: stationaire drukverdeling
2000011003	03	Grn	2	3		Geen toegevoegde waarde vanwege zwakke winden	
2000011112	24	Drp	4	1			Situatie: vlak lagedrukgebied, weinig gradient over groot gebied Veel gebiedjes met groene pijltjes. Alleen rond 40N40W duidelijk te interpreteren (2D-VAR beter)
2000011112	26	Drp	1,zadelvlak	1			zeer weinig gradient, Prescat lijkt iets beter in patroon te passen
2000011121	12	Drp	3	3			Geen waarn., Prescat lijkt realistischer
2000011200	03	Drp	4	2	nauwkeurige positionering depressiekern		Situatie: Kern van een depressie Geen waarn, Prescat onrealistisch, 2D-VAR moet juist zijn
2000011200	12	Drp	1	2	2D-VAR legt zadelpunt duidelijker vast Prescat wind waait tegen de gradient in		
2000011200	14	Drp	4	2	2D-VAR legt hogedrukcentrum nauwk. vast Prescat wind waait tegen de gradient in		
2000011221	16	Nlt	4	2	Nauwk. bepaling vore-as en afgesnoerd laagje	2D-VAR duidelijk beter Prescat fout op noordflank vore	Situatie: langerekte vore met klein afgesnoerd kerntje
2000011300	05	Nlt	3,rug	3			Beide methodes min of meer fout 2D-VAR over groter gebied
2000011303	08	Nlt	3,zadelvlak	3			Minimaal verschil in het hart v/h zadelgebied niet aan te geven welke methode beter is
2000011312	13	Vrg	3,trog	1	bepaling as trogvitloper	weinig verschil, weinig gradient structuur Prescat wat beter	
2000011315	07	Vrg	1,opvullend	2			2D-VAR winden ogen wat realistischer in het betrokken gebied, geen waarn.
20000115??	04	Grn	3	3		Geen van beide goed bruikbaar	Geen waarn., op basis wolkenband krijgt 2D-VAR evt. voordeel twijfel

Table 3.3: Findings of the meteorologists (continued)

DTG	MSG NR	MET	Class.	Beoord.	Nut		Opmerking(en)
					hoe te gebruiken	verschil in gebruik	
2000011615	06	Grn	3	3	Beide niet bruikbaar		Situatie: scherpe trog, geen waarn.
2000011615	10	Grn	2	2	Analyse stormveld, gaten dichten tussen SHIPS	2D-VAR veel beter,scherpe gradient en bevestigende waarnemingen	Situatie: ontwikkelend systeem met sterke drukgradient
2000012500	10	Grn	3	1	Operationeel van weinig betekenis	Prescat beter voor bepaling ligging zadelgebied	Prescat beter op basis isobarenpatroon+waarn.
2000012512	17	Slk	3	2	Voor analyse + FG	Ja, zie A	Situatie: front of trog, grote vectoren kleine vec rond zwakke rug oost v. laag
2000012515	08	Slk	2	3	Marginale verschil		Situatie: lagedruk flow
2000012521	11	Slk	1,opvullend	3	weinig additionele waarde		
2000012600	02	Slk	1,zw. rug	3	geen additionele info		Aanpassen drempelwaarde
2000012600	07	Slk	1,zadelvlak	3	geen additionele info		Dit is ruis
2000012712	21	Vrg	3,rug	2	nadere specificatie ligging rug-as	Prescat winden onjuist	
2000012815	03	Grn	1	2	Bepaling gradient in data-arm gebied	Prescat verwerpen op basis analyse-continuiteit	Situatie: opvullend systeem
2000012815	05	Grn	1	3	Onbelangrijk		Situatie: zwakke zadelconstructie
2000012900	06	Grn	3	1	Geen van beide is helder. Lastig		Geen waarn., NO wind past best bij analyse maar in tegenspraak met scatterometer-oplossingen Prescat best op basis uitwaaierende golven uit het noorden
2000012903	06	Grn	3	3	Geen operationeel belang		Situatie: scherpe rug/anticyclonaal zadel
2000013100	03	Grn	3,rug	1	Niet interessant gebied, lage snelheden		

Table 3.4: Findings of the meteorologists (continued)

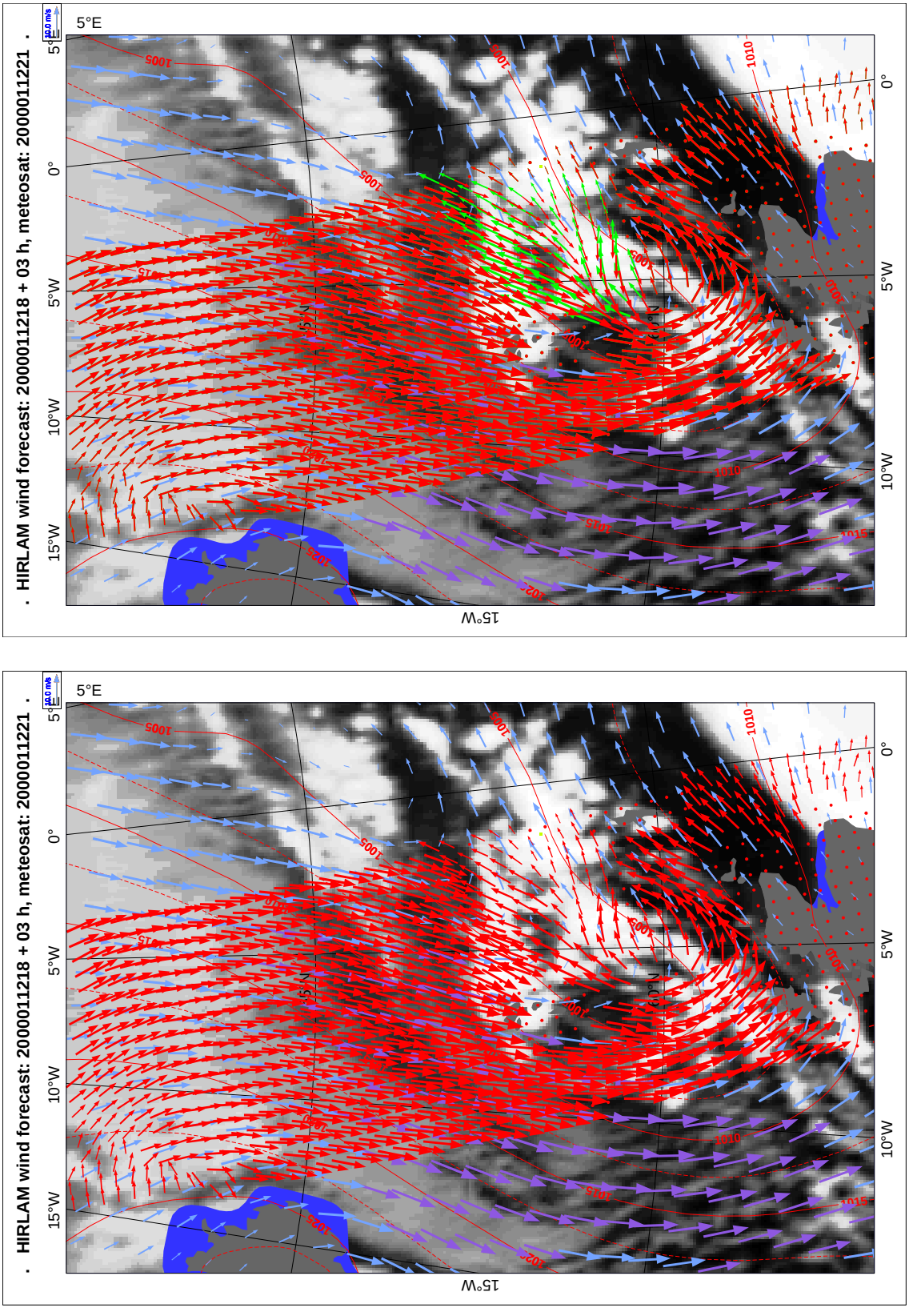

Figure 3.12: Low-pressure system north of Scotland, 2DVAR solution (right panel) is more consistent than PRESCAT. Example of the wind products noted as analysis tool for the meteorological offices of Iceland and the UK

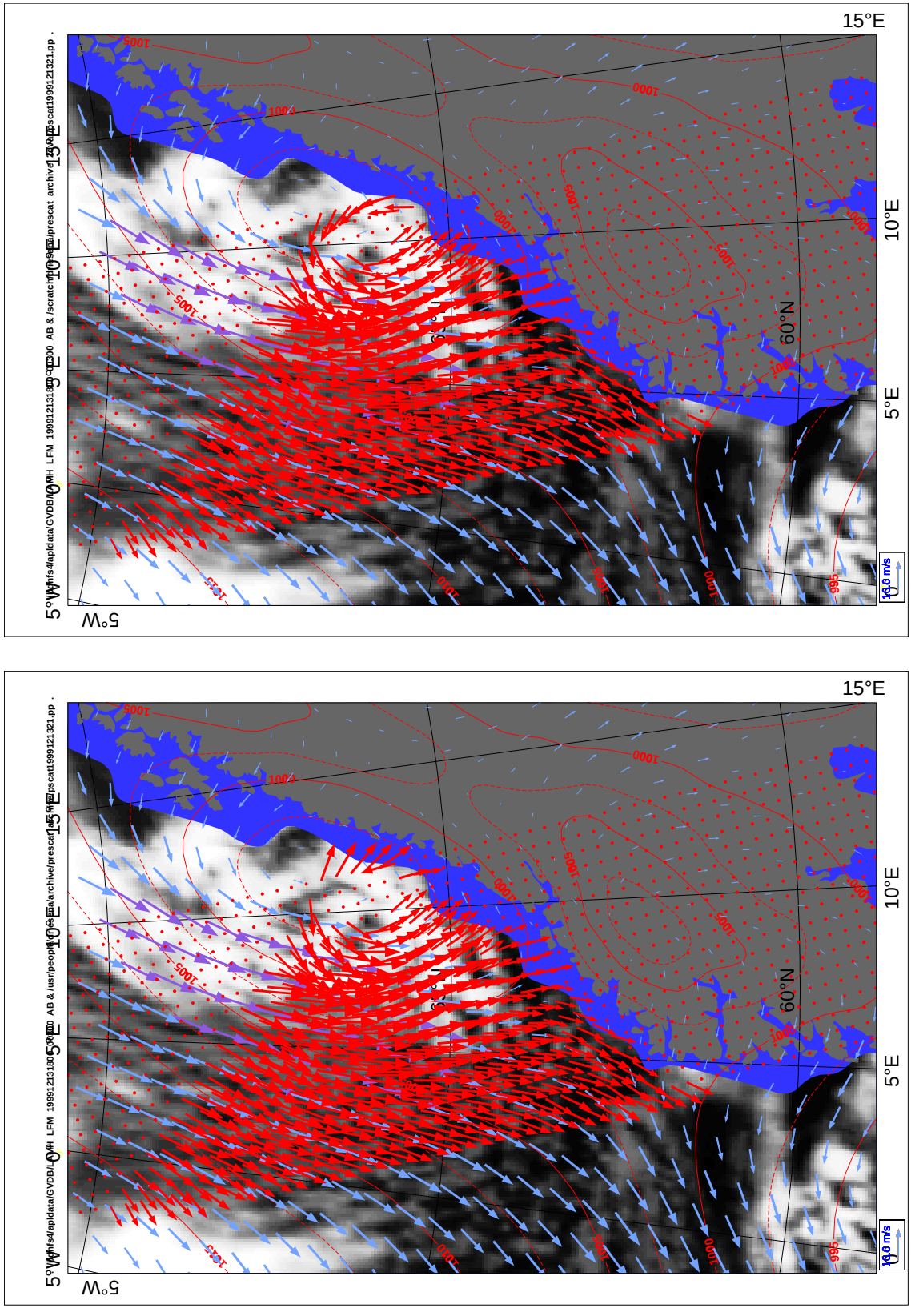

Figure 3.13: Polar low near the Norwegian West coast, it shows the improved ability of 2D-VAR (right panel) over PRESCAT to remove ambiguities in a meteorologically consistent way. Example of wind products noted as useful for meteorological analysis at the Norwegian meteorological office.

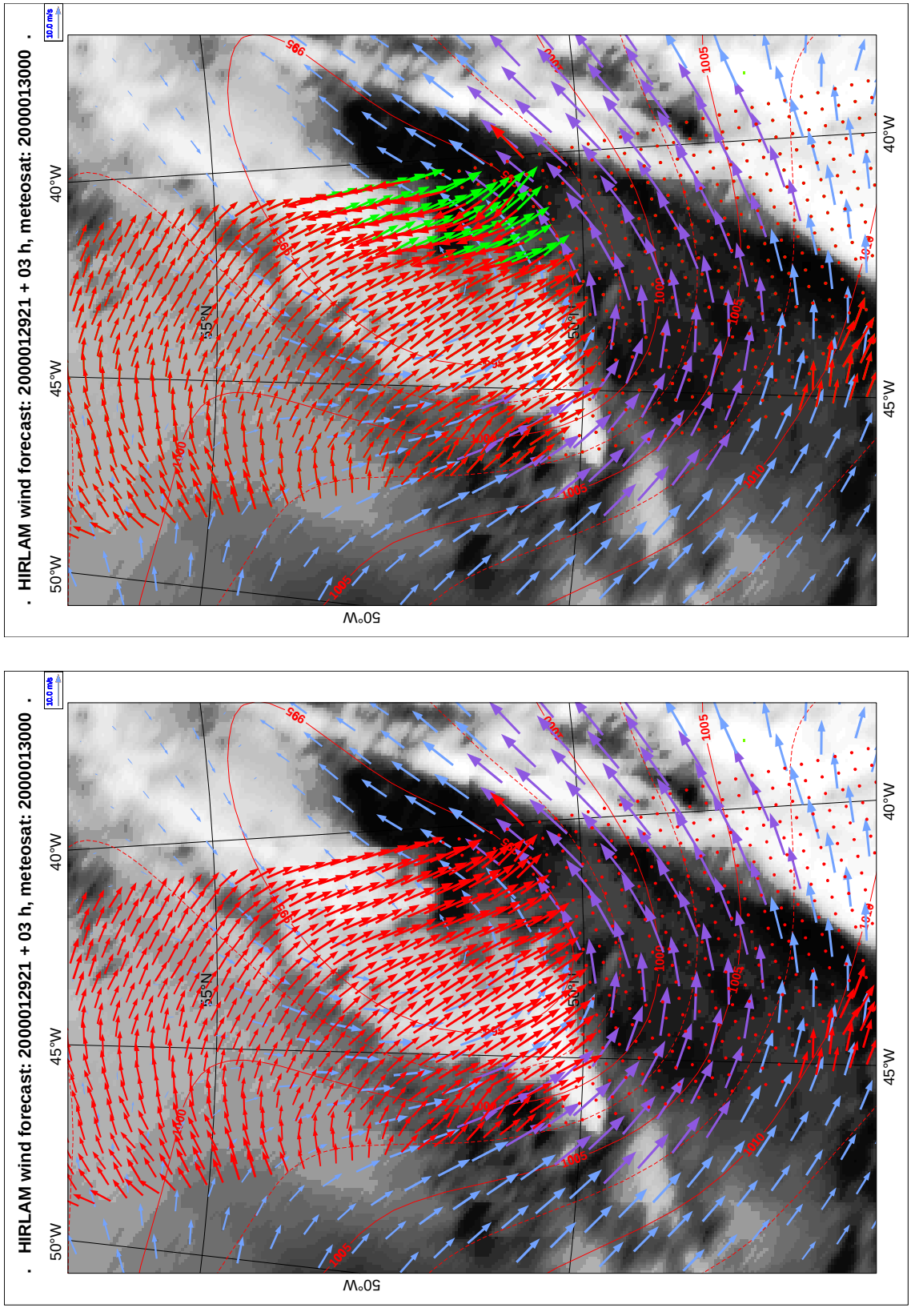

Figure 3.14: Trough of low pressure in the northern Atlantic. PRESCAT typically enforces wind field continuity (left panel), 2D-VAR contributes too much weight to the background field (right panel). Example of a more consistent wind field solution that can be attained by PRESCAT over 2D-VAR under this type of condition.

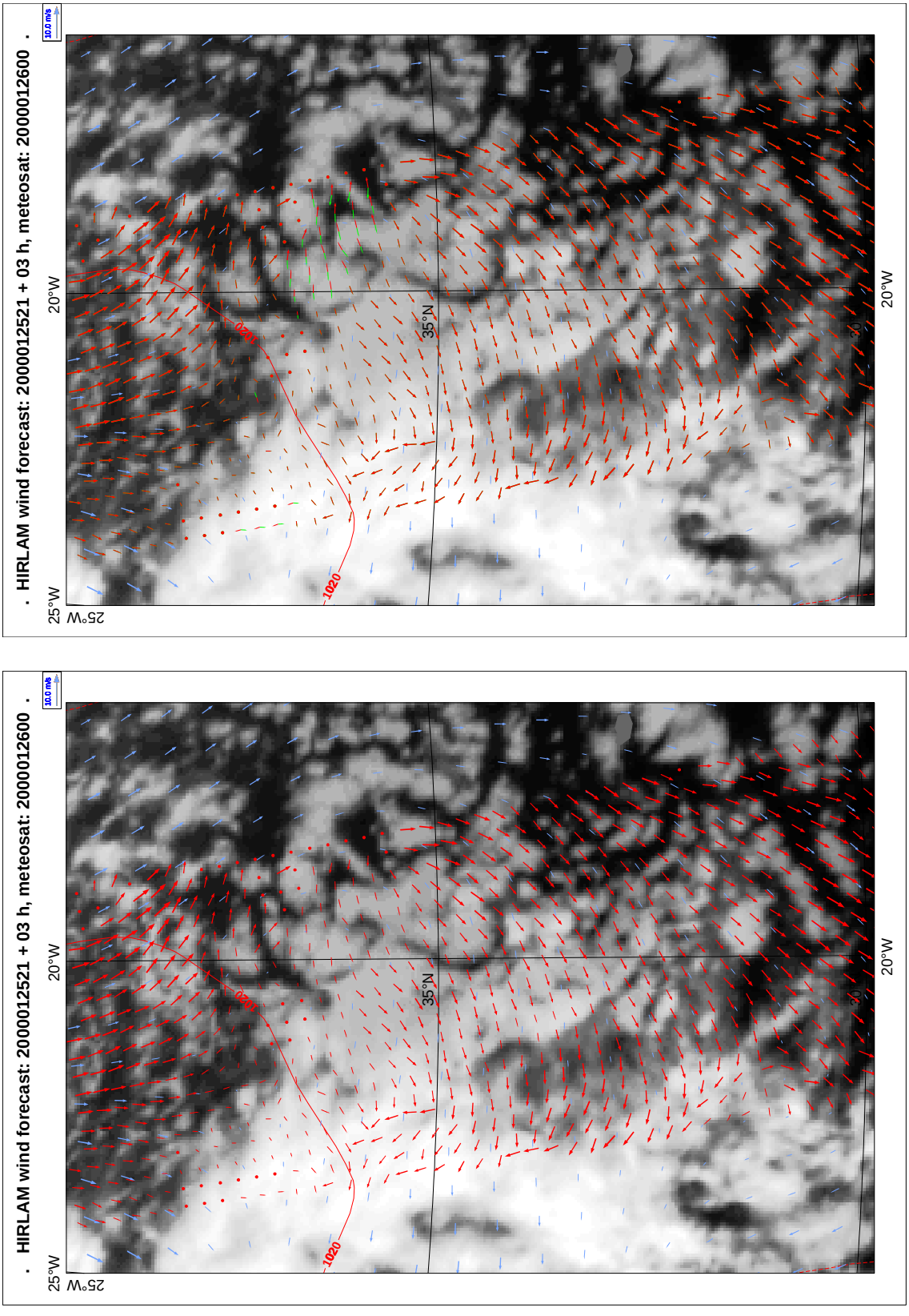

Figure 3.15: Stationary situation with weak winds, rated by the meteorologist as noise.

Chapter 4

Conclusions and recommendations

From the results of chapter 3 in this report we can draw following conclusions:

- In data-dense areas 2D-VAR is able to fit observed vortices absent in the background field.
- Observation grouping may have a beneficial effect on ambiguity removal near fronts.
- 2D-VAR shows both strengths and weaknesses after validation w.r.t. PRESCAT.
- An objective comparison test against an absolute reference has resulted in a favourable score for PRESCAT (55%-45%) compared to 2D-VAR in cases when both methods differ in their ambiguity removal solution.
- The subjective analysis of significantly different cases by KNMI meteorologists favours 2D-VAR.
- 2D-VAR is better at solving the ambiguity problem for weather systems in different stages of their development
- PRESCAT is better at selecting the right ambiguity in situations near fronts, troughs and ridges.
- In a substantial number of cases (37%) meteorologists were not able to make a clear choice on which of the ambiguity removal methods is better, 2D-VAR or PRESCAT.
- Wind products based on scatterometer winds contain small-scale information that is of added value to the meteorologist.

Recommendations

- In the analysis of the implementation of the 2D-VAR scheme we noted that the spatial filtering characteristics were not as expected. In particular, analysis increments seem to have too little rotation. Further investigation of the behaviour of 2D-VAR is necessary, especially in data-sparse situations, in order to utilise the full potential of 2D-VAR
- The impact of observation grouping could be look at more closely
- The objective comparison between PRESCAT and 2D-VAR could be repeated but for a longer period of time and more geographical areas to filter out possible statistical effects.
- Investigate the use of situation dependent covariance functions. They may lead to better performance of 2D-VAR.

Future developments

The 2D-VAR scheme is going to be used in a comparison study with a similar AR-scheme developed at IFREMER to assess their relative performances and ascertain whether it is a suitable candidate for implementation in the OSI SAF processing chain.

Outlook

With the advent of new scatterometers that have scanning strategies different from ERS-scatterometers, ambiguity removal remains a topic of continuing development and importance.

The NSCAT scatterometer although being lost is still interesting from a scientific point of view. NSCAT has six antennae that provide both horizontal and vertical polarisation measurements that result in four different σ^0's from each target over the ocean. The inversion leads to up to four ambiguous wind vectors per node which aggravates the ambiguity problem compared to ERS. 2D-VAR can be used to develop an NSCAT cost function and to investigate the ambiguity removal problem for this type of scatterometer.

Another scatterometer that has recently been launched is QuikSCAT. QuikSCAT is the first scatterometer with a rotating pencil beam. It has a wide swath of approximately 1800 km. Since February 1999 a BCRS-sponsored project is taking

place at KNMI to investigate an early operational QuikSCAT wind product. 2D-VAR can be a useful tool in the development of such a wind product for QuikSCAT.

With the availability of QuikSCAT the coverage problem for surface wind observations is reduced considerably. In the near future meteorologists can conttribute to the fine tuning and evaluation of the quality control of the data from QuikSCAT. This will facilitate the possible operational use of a QuikSCAT wind product.

As a final remark we note that 2D-VAR is a useful learning tool. Indeed, apart from applications in ambiguity removal it may be used to investigate other aspects of variational analysis of meteorological fields.

Appendix A

The observational method

The observational method is an empirical method to obtain error covariance functions from observation-minus-background wind departures. It involves the computation of mean covariances, averaged over a longer period of time. For a detailed description of the method the reader is referred to Hollingsworth and Lönnberg [6] and Bartello and Mitchell [1]. Here a description is given of how the observational method is used for 2D-VAR with ERS-scatterometer observations.

The method starts by computing observation-minus-background wind departures

$$\mathbf{v^o} - \mathbf{v}^b = \begin{pmatrix} u^o - u^b \\ v^o - v^b \end{pmatrix} \tag{A.1}$$

The background wind is interpolated from NWP grid point locations to the scatterometer nodes. If we have wind departures at positions $\mathbf{i}$ and $\mathbf{j}$ we can define for a mean error covariance matrix

$$\begin{aligned} \mathbf{F_{ij}} &= \mathbf{B_{ij}} + \mathbf{O_{ij}} \\ &= \langle (\mathbf{v}^o - \mathbf{v}^b)_\mathbf{i}, (\mathbf{v}^o - \mathbf{v}^b)_\mathbf{j} \rangle \\ &= \langle [(\mathbf{v}^o - \mathbf{v}^t) - (\mathbf{v}^b - \mathbf{v}^t)]_\mathbf{i}, [(\mathbf{v}^o - \mathbf{v}^t) - (\mathbf{v}^b - \mathbf{v}^t)]_\mathbf{j} \rangle \\ &= \langle \mathbf{e_i}^o \mathbf{e_j}^o - \mathbf{e_i}^o \mathbf{e_j}^b - \mathbf{e_i}^b \mathbf{e_j}^o + \mathbf{e_i}^b \mathbf{e_j}^b \rangle \end{aligned} \tag{A.2}$$

where $\mathbf{e}$ denotes deviation from the true value (i.e. wind error) and $\langle\rangle$ indicates averaging over many realisations. We assume that the observation error is not spatially correlated, i.e. $\mathbf{e_i}^o \mathbf{e_j}^o = 0$ if $\mathbf{i} \neq \mathbf{j}$, which is valid if we take the resolution of the scatterometer observations lower than the scatterometer footprint (50 km). We also assume that the observation error is not correlated with the background error ($\mathbf{e_i}^o \mathbf{e_j}^b = \mathbf{e_i}^b \mathbf{e_j}^o = 0$). This yields $\mathbf{F_{ij}} = \mathbf{B_{ij}}$ for $\mathbf{i} \neq \mathbf{j}$ (see equation 2.11).

At zero separation the total wind error variance is found from

$$\lim_{\mathbf{r_{ij}}\to 0} \mathbf{F}_{|\mathbf{i}-\mathbf{j}|} = \mathbf{E_F}^2 = \mathbf{E}_b^2 + \mathbf{E}_o^2 \tag{A.3}$$

The total wind error variance $\mathbf{E_F}^2$ is a constant under the assumption of homogeneity and consists of an observational and a background part. The total wind error covariance tensor can be expressed in terms of the observation-minus-background wind difference components which gives

$$\mathbf{F}_{|\mathbf{i}-\mathbf{j}|} = \begin{pmatrix} \langle u_i, u_j \rangle & \langle u_i, v_j \rangle \\ \langle v_i, u_j \rangle & \langle v_i, v_j \rangle \end{pmatrix} \tag{A.4}$$

with

$$\lim_{\mathbf{r_{ij}}\to 0} \mathbf{F}_{|\mathbf{i}-\mathbf{j}|} = \begin{pmatrix} E_u^2 & 0 \\ 0 & E_v^2 \end{pmatrix} \tag{A.5}$$

and

$$\begin{aligned} E_u^2 &= E_{bu}^2 + E_{ou}^2 \\ E_v^2 &= E_{bv}^2 + E_{ov}^2 \end{aligned} \tag{A.6}$$

The next step is to apply the assumptions of homogeneity and isotropy. These assumptions make the error covariances invariant under rotation of the frame of reference. As a result, when computing an arbitrary error covariance, the frame of reference can be rotated over an angle α so that the component covariances may be expressed in terms of a longitudinal component l and a transverse component t (see fig.A.1).

$$\begin{aligned} l &= u cos\alpha + v sin\alpha \\ t &= -u sin\alpha + v cos\alpha \end{aligned} \tag{A.7}$$

with which the error covariance tensor becomes

$$\mathbf{F}_{|\mathbf{i}-\mathbf{j}|} = \begin{pmatrix} \langle l_i, l_j \rangle & 0 \\ 0 & \langle t_i, t_j \rangle \end{pmatrix}. \tag{A.8}$$

Here $\langle l_i, t_j \rangle = \langle t_i, l_j \rangle = 0$ due to the assumption of homogeneity and isotropy. Because of homogeneity the total wind error variance becomes

$$\lim_{\mathbf{r_{ij}}\to 0} \mathbf{F}_{|\mathbf{i}-\mathbf{j}|} = E_u^2 + E_v^2 = E_l^2 + E_t^2 = E_{bl}^2 + E_{bt}^2 + E_{ol}^2 + E_{ot}^2 \tag{A.9}$$

In addition isotropy leads to

$$E_l^2 = E_t^2 = \frac{1}{2}|\mathbf{E}_F|^2 \tag{A.10}$$

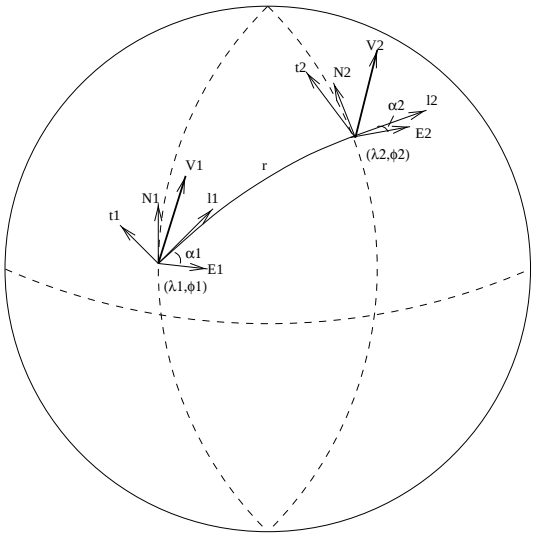

Figure A.1: Definition of longitudinal and transverse wind components.

The observational method proceeds by computing a histogram of departure covariances as a function of separation distance. The departure covariances are averaged per bin. For the application in 2D-VAR a model function f is fitted through the mean covariances F_i by means of a least squares fit. In the least squares fit the function

$$\chi^2 = \sum_{i=1}^{N} \left(F_i - f(r_i)\right)^2 W_i \tag{A.11}$$

is minimized where W_i is a weight factor that represents the number of error covariances in the i^{th} bin. The function used is the Fourier-Bessel series

$$f(r_i) = \sum_{j=0}^{M} a_j J_0\left(\frac{k_j r_i}{r_0}\right) \tag{A.12}$$

with J_0 being the Bessel function of the first kind and integer order zero. The k_j are the roots of a Bessel function that follow from the boundary condition specified at the distance r_0. A suitable boundary condition can be defined when looking at the mean covariance data. If the covariance data becomes small at large distances and actually goes to zero the condition

$$f(r_0) = 0 \tag{A.13}$$

can be applied in which case the k_j are the roots of J_0. If on the other hand the mean covariances become small at large distances, do not go to zero but the gradient

in the data does, the condition

$$\frac{\partial}{\partial r} f(r_0) = 0 \tag{A.14}$$

can be applied, which implies that the k_j are the roots of J_1. The number of terms M used in the series is determined by the wave number that corresponds to the smallest resolved scale in the 2D-VAR analysis grid.

With the assumption that observation errors are not spatially correlated it is possible to separate the observation error variance from the background error variance. To do this the model function is extrapolated to zero intercept which results in $\mathbf{E}^2(0)$. With the known value for the mean error vector variance $\mathbf{E_F^2}$

$$\mathbf{E}_b^2 = \mathbf{E}^2(0) \tag{A.15}$$

and equations (A.3) and (A.10) the observation and background error variance and the background error component variances can be determined. The model function obtained in this way can be used in 2D-VAR if it is positive-definite which requires positive spectral coefficients (Gandin [4]).

The motivation for the selection of the Fourier-Bessel series as model function lies in the fact that the Fourier-Bessel series, also known as a discrete Hankel transform, is equivalent to the discrete 2D Fourier transform of a radial function (of distance). As a result the coefficients of the model function are proportional to the spectral representation of the background error covariances used in 2D-VAR.

Latitude dependence

For the regional implementation scatterometer data from latitudes of 30N-90N are used. In a global implementation separate covariance functions would have to be derived for the whole globe. For the tropics due to the different nature of atmospheric dynamics. In the southern hemisphere mainly due to the difference in land mass distribution compared with the northern hemisphere.

Appendix B

Wind departures on a sphere

To compute homogeneous and isotropic two-point auto-covariances we have to determine the longitudinal and transverse components of wind departure fields on a sphere. To do this we need

- the great circle distance between two points
- the orientation of the separation vector relative to the local East and North at each point

The latter because wind component departures u and v are defined relative to the local tangent plane to the Earth. The situation for two arbitrary point locations is depicted in fig. A.1. If we consider the Earth to be a perfect sphere we can express any location $\mathbf{r}$ on the sphere using spherical coordinates as the position vector

$$\mathbf{r} = (x, y, z) \tag{B.1}$$

with

$$\begin{aligned} x &= a \cos\lambda \cos\theta \\ y &= a \sin\lambda \cos\theta \\ z &= a \sin\theta \end{aligned} \tag{B.2}$$

where a is the radius of the Earth and λ and θ are longitudes and latitudes respectively. The angle γ between two position vectors $\mathbf{r}_1$ and $\mathbf{r}_2$ is expressed as

$$\gamma = \arccos \frac{\mathbf{r}_1 \mathbf{r}_2}{|\mathbf{r}_1|\,|\mathbf{r}_2|} \tag{B.3}$$

The great circle distance d between two arbitrary points is

$$\begin{array}{rcll} d & = & a\gamma & \\ & = & a\arccos(& \cos\lambda_1\cos\theta_1\cos\lambda_2\cos\theta_2 \quad + \\ & & & \sin\lambda_1\cos\theta_1\sin\lambda_2\cos\theta_2 \quad + \\ & & & \sin\theta_1\sin\theta_2 \qquad\qquad\qquad\quad) \end{array} \tag{B.4}$$

and the separation vector (figure B.1) is

$$\begin{array}{rcll} \mathbf{r}_{12} & = & \mathbf{r}_2 - \mathbf{r}_1 & \\ & = & a(& \cos\lambda_2\cos\theta_2 - \cos\lambda_1\cos\theta_1 \quad , \\ & & & \sin\lambda_2\cos\theta_2 - \sin\lambda_1\cos\theta_1 \quad , \\ & & & \sin\theta_2 - \sin\theta_1 \qquad\qquad\quad) \end{array} \tag{B.5}$$

For the orientation of the separation vector relative to East in the local tangent plane we consider the unit outward normal which can be expressed as

$$\mathbf{n} = \frac{\mathbf{r}_\lambda \otimes \mathbf{r}_\theta}{|\mathbf{r}_\lambda \otimes \mathbf{r}_\theta|} \tag{B.6}$$

where $\otimes$ denotes cross product and the subscript denotes differentiation. The unit outward normal is the cross product of the eastward and northward unit vector that span up the local tangent plane.
The unit vector for East and North are

$$\begin{array}{rcl} \mathbf{n}_{east} & = & (-\sin\lambda, \cos\lambda, 0) \\ \mathbf{n}_{north} & = & (-\cos\lambda\sin\theta, -\sin\lambda\sin\theta, \cos\theta) \end{array} \tag{B.7}$$

The orientation of the separation vector can be found if we project it onto the local tangent plane (fig.B.1)

$$P\mathbf{r}_{12} = (\mathbf{r}_{12}.\mathbf{n}_{\mathbf{north}})\mathbf{n}_{\mathbf{north}} + (\mathbf{r}_{12}.\mathbf{n}_{\mathbf{east}})\mathbf{n}_{\mathbf{east}} \tag{B.8}$$

The angle between the separation vector and the local East then follows from

$$\alpha = \arccos \frac{P\mathbf{r}_{12}.\mathbf{n}_{\mathbf{east}}}{\sqrt{\mathbf{r}_{12}.\mathbf{n}_{\mathbf{north}} + \mathbf{r}_{12}.\mathbf{n}_{\mathbf{east}}}} \tag{B.9}$$

Finally we have for the longitudinal and transverse wind component departures

$$\begin{array}{rcrcl} l & = & u\cos\alpha & + & v\sin\alpha \\ t & = & -u\sin\alpha & + & v\cos\alpha \end{array} \tag{B.10}$$

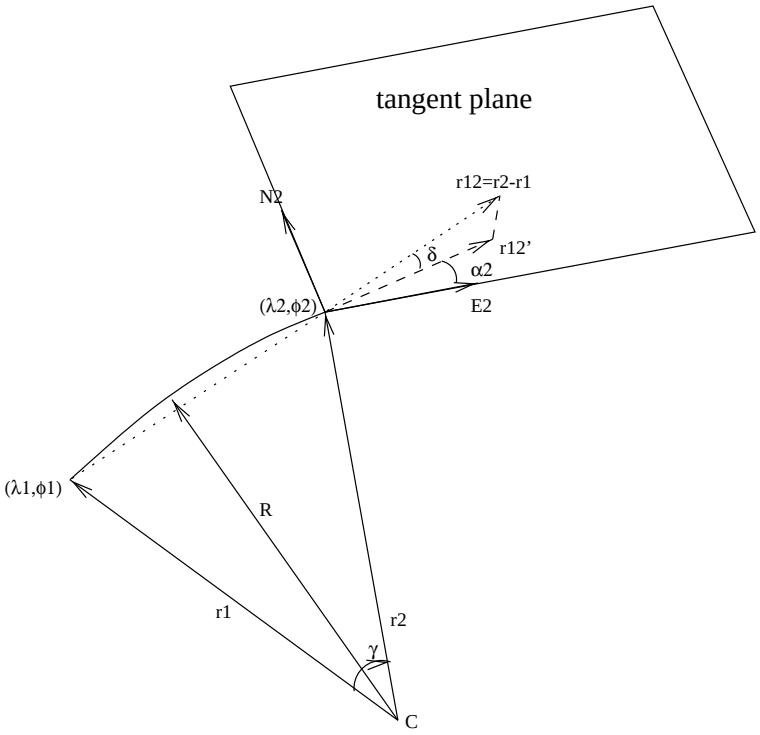

Figure B.1: Projection of the separation vector on the tangent plane.

Appendix C

Quasi-geostrophic error covariance functions

The concept behind 2D-VAR is that physical laws that constrain the spatial structure of the wind help in solving the scatterometer ambiguity problem. This spatial structure is incorporated in the empirical covariance functions. An alternative to these empirical covariance functions are the so-called quasi-geostrophic covariance functions which are parametric. In the atmosphere above the boundary layer synoptic flow is in approximate geostrophic balance. This balance constrains the structure of the wind field. In the boundary layer the geostrophic balance is less pronounced due to friction. This fact can be used to derive quasi-geostrophic covariance functions from the equations of motion.

To define quasi-geostrophic covariance functions we follow Buell [2] and start with the geostrophic wind equations on a isobaric surface

$$u = -\frac{g}{f}\frac{\partial h}{\partial y}, \quad v = \frac{g}{f}\frac{\partial h}{\partial x} \tag{C.1}$$

The two-point covariances based on these equations are

$$b^{uu}_{i,j} = \frac{g^2}{f_i f_j}\frac{\partial^2}{\partial y^2} b^{hh}_{i,j} \tag{C.2}$$

$$b^{vv}_{i,j} = \frac{g^2}{f_i f_j}\frac{\partial^2}{\partial x^2} b^{hh}_{i,j} \tag{C.3}$$

$$b^{uv}_{i,j} = \frac{g^2}{f_i f_j}\frac{\partial^2}{\partial y \partial x} b^{hh}_{i,j} \tag{C.4}$$

$$b^{vu}_{i,j} = \frac{g^2}{f_i f_j}\frac{\partial^2}{\partial x \partial y} b^{hh}_{i,j} \tag{C.5}$$

The homogeneous and isotropic longitudinal and transverse covariances can be found by rotating the frame of reference. Using radial derivatives we find

$$b^{ll}_{|i-j|} = -\frac{g^2}{f_i f_j}\frac{1}{r}\frac{\partial}{\partial r} b^{hh}_{|i-j|} \tag{C.6}$$

$$b^{tt}_{|i-j|} = -\frac{g^2}{f_i f_j}\frac{\partial^2}{\partial r^2} b^{hh}_{|i-j|} \tag{C.7}$$

Homogeneous and isotropic covariance functions can be split in a variance part and a correlation function

$$b = E^2 \rho(r) \tag{C.8}$$

The variance part is constant (homogeneity) and the equal for the component covariance functions. The correlation part is a circular symmetric function of distance only and is also known as *structure function*. From equation (C.6) and (C.7) it follows that the longitudinal and transverse covariances are related. Using (C.8) we obtain

$$\rho^{tt} = \rho^{ll} + c_g r \frac{\partial \rho^{ll}}{\partial r} \tag{C.9}$$

Here c_g is a tuning parameter with which the amount of geostrophic adherence can be controled. For $c_g = 1$ the component covariance functions are geostrophically related.

The next step is to define an analytical model function. We selected a function that is positive definite under Fourier transform.

$$\rho^{hh} = e^{-\frac{r^2}{2L^2}} \tag{C.10}$$

With this function it follows that

$$\rho^{ll} = \frac{-1}{L^2} e^{-\frac{r^2}{2L^2}} \tag{C.11}$$

and

$$\rho^{tt} = \frac{-1}{L^2}(1 - c_g \frac{r^2}{L^2}) e^{-\frac{r^2}{2L^2}} \tag{C.12}$$

For the application in 2D-VAR we used the variance found from the empirical covariance functions. Apart from c_g the analytical structure functions contain a tuneable parameter in the form of the characteristic length scale L. We note that changing the length scale results in a change in the variance by a factor $(\frac{L}{L'})^2$. The tuning

parameters c_g and L may prove to be an advantage to find a solution in individual cases and situation-dependent covariance functions may also help the tuning of 2D-VAR in general.

Bibliography

[1] P. Bartello and H.L. Mitchell. *A continuous three-dimensional model of short-range forecast error covariances. Tellus 44 A*, pages 217–235, 1992.

[2] C. Eugene Buell. *Correlation Functions for Wind and Geopotential on Isobaric Surfaces. Journal of Applied Meteorology*, pages 51–59, 1972.

[3] A. Cavanie and P. Lecomte. *Volume 1 - Study of a method to de-alias winds from ERS-1 data. Volume 2 - Wind retrieval and de-aliasing subroutines.* Technical report, ESTEC Noordwijk, The Netherlands., 1987. Final rep. ESA contract No 6874/87/CP-I(sc).

[4] L.S. Gandin. *Objective Analysis of Meteorological Fields.* Israel Program for Scientific Translation, 1965.

[5] J. Ch. Gilbert and C. Lemarechal. *Some numerical experiments with variable storage quasi-Newton algorithms. Mathematical Programming, B25*, pages 407–435, 1989.

[6] A. Hollingsworth and P. Lonnberg. *The statistical structure of short-range forecast errors as determined from radiosonde data. Part I: The wind field. Tellus 38 A*, pages 111–136, 1986.

[7] Mariken Homleid and Lars-Anders Breivik. *Preparations for the assimilation of ERS-1 surface wind observations into numerical weather prediction models.* Technical report, The Norwegian Meteorological Institute, 1993.

[8] A.C. Lorenc. *Analysis methods for numerical weather prediction. Quarterly J.R. Met. Soc. 112*, pages 1177–1194, 1986.

[9] I.M. Navon and D.M. Legler. *Conjugate Gradient Methods for Large-Scale Minimization in Meteorology. Monthly Weather Review, 115*, pages 1479–1502, 1987.

[10] D. Offiler. *ERS-1 Wind Retrieval Algorithms, U.K. Meteorolgical O. 19 Branch Memorandum No.86.* Technical report, Meteorological Office, Bracknell, England., 1987.

[11] W.H. Press, B.P. Flannery, S.A. Teukolsky, and W.T. Vetterling. *Numerical Recipes.* Cambridge University Press, 1989.

[12] Harald Schyberg and Lars-Anders Breivik. *Two dimensional variational analysis of ocean surface winds, No. 42.* Technical report, Norwegian Meteorological Institute, Oslo, 1996.

[13] Harald Schyberg and Lars-Anders Breivik. *Ambiguity Removal Evaluation, No. 64.* Technical report, Norwegian Meteorological Institute, Oslo, 1998.

[14] A. Stoffelen. *Scatterometry (http://pablo.ubu.ruu.nl/p̃roefschrift/01840669/inhoud.htm).* PhD. thesis, 1998.

[15] A. Stoffelen and D. Anderson. *Scatterometer data interpretation: Measurement space and Inversion. J. Atmos. Oceanic Technol., 14(6)*, pages 1298–1313, 1997.

[16] A. C. M. Stoffelen and D. L. T. Anderson. *Ambiguity Removal and assimilation of scatterometer data. Q.J. Roy. Meteorol. Soc., 123)*, pages 491–518, 1997.

[17] A. C. M. Stoffelen and D. L. T. Anderson. *Scatterometer data interpretation: Estimation and Validation of the transfer function CMOD4. J. Geophys. Res., 102(C3)*, pages 5767–5780, 1997.

[18] Ad Stoffelen and Paul van Beukering. *Improved backscatter processing and impact of tandem ERS winds on HIRLAM.* Technical report, HIRLAM report nr.31, IMET, Ireland, 1997.

[19] J-N. Thepaut, P. Courtier, and R.H. Hoffman. *Use of dynamical information in 4D variational assimilation. Variational assimilations, with special emphasis on three-dimensional aspects, Workshop proceedings*, pages 237–269, 1992.